EUROPEAN RESPIRATORY *journal*

FLAGSHIP SCIENTIFIC JOURNAL OF ERS

Early View

Original article

Endothelial eNAMPT Amplifies Preclinical Acute Lung Injury: Efficacy of an eNAMPT-Neutralising mAb

Hector Quijada, Tadeo Bermudez, Carrie L. Kempf, Daniel G. Valera, Alexander N. Garcia, Sara M. Camp, Jin H. Song, Evelyn Franco, Jessica K. Burt, Belinda Sun, Joseph B. Mascarenhas, Kimberlie Burns, Amir Gaber, Radu C. Oita, Vivian Reyes Hernon, Christy Barber, Liliana Moreno-Vinasco, Xiaoguang Sun, Anne E. Cress, Diego Martin, Zhonglin Liu, Ankit A. Desai, Viswanathan Natarajan, Jeffrey R. Jacobson, Steven M. Dudek, Christian Bime, Saad Sammani, Joe G. N. Garcia

Please cite this article as: Quijada H, Bermudez T, Kempf CL, *et al*. Endothelial eNAMPT Amplifies Preclinical Acute Lung Injury: Efficacy of an eNAMPT-Neutralising mAb. *Eur Respir J* 2020; in press (https://doi.org/10.1183/13993003.02536-2020).

Endothelial eNAMPT Amplifies Preclinical Acute Lung Injury: Efficacy of an eNAMPT-Neutralizing mAb

Hector Quijada[1^], Tadeo Bermudez[1^], Carrie L. Kempf[1], Daniel G. Valera[1], Alexander N. Garcia[2], Sara M. Camp[1], Jin H. Song[1], Evelyn Franco[1], Jessica K. Burt[1], Belinda Sun[3], Joseph B. Mascarenhas[1], Kimberlie Burns[1], Amir Gaber[1], Radu C. Oita[1], Vivian Reyes Hernon[1], Christy Barber[4], Liliana Moreno-Vinasco[1], Xiaoguang Sun[1], Anne E. Cress[5], Diego Martin[6], Zhonglin Liu[4], Ankit A. Desai[7], Viswanathan Natarajan[8], Jeffrey R. Jacobson[8], Steven M. Dudek[8], Christian Bime[1], Saad Sammani[1#], Joe G. N. Garcia[1#§]

^ Co-first authors; # Co-senior authors, § Corresponding author

Joe G. N. Garcia, MD
University of Arizona Health Sciences
Office Phone: (520) 626-1197
skipgarcia@email.arizona.edu

Authors affiliations:
Department of Medicine[1], Department of Radiation Oncology[2], Department of Pathology[3], Department of Medical Imaging[4], Department of Cellular and Molecular Medicine[5], University of Arizona Health Sciences, Tucson, AZ; Department of Diagnostic Radiology[6], McGill University, Montreal, QC; Department of Medicine[7], Indiana University, Indianapolis IN; Department of Medicine[8], University of Illinois Chicago, Chicago IL.

Author Contributions:
JGNG, SS – conception and design of the work, the analysis and interpretation of data for the work, the drafting and revision of the manuscript, approval of final version to be published
CB, AEC, ZL, DM – conception and design of the work, the analysis and interpretation of data for the work, critical revision of key intellectual content and approval of final version to be published.
TB, SMC, ANG, CLK, HQ, DGV, JS – collection and analysis of data, revision of the manuscript, and approval of the final version to be published
CB, KB, JKB, AAD, SMD, EF, AG, JRJ, JM, LMV, VN, RCO, VRH, BS, XS – collected data and assisted with processing and manuscript revision

****Funding**: This work was supported by the NIH/NHLBI grants P01HL126609, R01HL094394, and P01HL134610
Running Title:* Endothelial eNAMPT is a Key Therapeutic Target in ARDS
****Keywords**: ARDS, eNAMPT, mAb, ALISS, DAMP
Descriptor Number: 4.1 ALI/ARDS: Biological Mechanisms

Word Count: 3,485 (<3,000 due to extensive data included and subsequent need for additional results and basic methods descriptions)

TAKE HOME MESSAGE

Underscoring the therapeutic potential for targeting the eNAMPT/TLR4 pathway in ARDS/VILI, a humanized eNAMPT-neutralizing monoclonal antibody (mAb) was highly effective in reducing the severity of ARDS in these dual complementary preclinical ARDS models.

ABSTRACT

Rationale: The SARS-CoV-2/COVID-19 pandemic has highlighted the serious unmet need for effective therapies that reduce ARDS mortality. We explored whether extracellular nicotinamide phosphoribosyltransferase (eNAMPT), a ligand for Toll-like receptor 4 and a master regulator of innate immunity and inflammation, is a potential ARDS therapeutic target. **Methods:** Wild type C57BL/6J or endothelial cell (EC)-c*NAMPT*$^{-/-}$ knockout mice (targeted EC *NAMPT* deletion) were exposed to either a lipopolysaccharide (LPS)-induced ("one-hit") or a combined LPS/ventilator ("two-hit")-induced acute inflammatory lung injury model. A NAMPT-specific mAb imaging probe (^{99m}Tc-ProNamptor^{TM}) was used to detect NAMPT expression in lung tissues. Either an eNAMPT-neutralizing goat polyclonal antibody (pAb) or a humanized monoclonal antibody (ALT-100 mAb) were utilized *in vitro* and *in vivo*. **Results:** Immunohistochemical, biochemical, and imaging studies validated time-dependent increases in NAMPT lung tissue expression in both preclinical ARDS models. Intravenous delivery of either eNAMPT-neutralizing pAb/mAb significantly attenuated

inflammatory lung injury (H & E staining, BAL protein, BAL PMNs, plasma IL-6) in both preclinical models. *In vitro* human lung EC studies demonstrated eNAMPT-neutralizing antibodies (pAb, mAb) to strongly abrogate eNAMPT-induced TLR4 pathway activation and EC barrier disruption. *In vivo* studies in wild type and EC-c*NAMPT*$^{-/-}$ mice confirmed a highly significant contribution of EC-derived NAMPT to the severity of inflammatory lung injury in both preclinical ARDS models. **Conclusions:** These findings highlight both the role of EC-derived eNAMPT and the potential for biologic targeting of the eNAMPT/TLR4 inflammatory pathway. In combination with predictive eNAMPT biomarker and *NAMPT* genotyping assays, this offers the opportunity to identify high-risk ARDS subjects for delivery of personalized medicine.

INTRODUCTION

The SARS-CoV-2/COVID-19 pandemic and the unprecedented numbers of deaths due to COVID-19-induced acute respiratory distress syndrome (ARDS) have dramatically highlighted multiple unmet needs for ARDS patients. These include the absence of validated ARDS biomarkers and the absence of effective FDA–approved ARDS pharmacotherapies to address the associated lethal multi-organ failure. Although insights into ARD/VILI pathobiology are limited, a key advance has been the appreciation of bacteria- and virus-induced activation of evolutionarily-conserved systemic inflammatory networks [1-3], releasing a “cytokine storm” that increases lung and systemic vascular permeability, organ edema, and multi-organ dysfunction [4-7] ultimately increasing COVID-19-ARDS and non-COVID-19 ARDS mortality [8-10]. The life-threatening organ dysfunction is caused by dysregulated host responses to infection

[6] mediated via interactions of pathogen-associated molecular patterns (PAMPs) and pattern recognition receptors (PRRs) that can also be activated by host nuclear, mitochondrial, and cytosolic proteins known as damage-associated molecular patterns (DAMPs). DAMPs are also released in response to danger signals such as hypoxia, cancer, trauma, and inhalation injury, thus potentially perpetuating a non-infectious inflammatory response [11].

We previously utilized preclinical multi-specie ARDS models coupled with genomic–intensive approaches [12, 13] to identify novel ARDS biomarkers and targetable pathways [12-18] and identified nicotinamide phosphoribosyltransferase (NAMPT) as a novel DAMP [19] and attractive ARDS target. We showed NAMPT expression to be highly induced by multiple ARDS-related stimuli including bacterial infection, hypoxia, shock, trauma, and excessive mechanical stress produced by mechanical ventilation [20-23]. Reduced expression of the gene encoding NAMPT (*NAMPT*) via siRNAs, miRNAs, and utilization of *NAMPT*$^{+/-}$ heterozygous mice, dramatically attenuated the severity of preclinical ARDS/VILI injury [17].

NAMPT is a cytozyme whose intracellular enzymatic activities (iNAMPT) regulate nicotinamide adenine dinucleotide (NAD) biosynthesis [24, 25], contributing to injury in a tissue- and cell-specific manner [26]. Our studies, however, much more strongly implicate secreted extracellular eNAMPT as the primary mechanism of NAMPT's contribution to inflammatory lung inury and the increased mortality of critically ill ARDS patients on mechanical ventilation [17, 19, 27]. eNAMPT is a master regulator of inflammatory networks via binding to the PRR, Toll-like receptor 4 (TLR4) [19], eliciting profound NFkB-mediated inflammatory cytokine release that increases vascular

permeability and multi-organ dysfunction directly linked to ARDS mortality [14, 28-30]. Two critical observations link NAMPT expression and function to human ARDS pathobiology. First, eNAMPT plasma levels alone [14, 31-33], or as part of an ARDS plasma biomarker panel [14, 31-33], are associated with ARDS severity and mortality. Secondly, *NAMPT* genetic variants that alter promoter activity in response to excessive mechanical stress [14, 22, 29, 30] and hypoxia [23] also confer increased ARDS susceptibility and mortality [14, 22, 29, 30].

In the current study, we explored the validation of eNAMPT as a viable ARDS therapeutic target in “one-hit” (LPS) and “two-hit” (LPS/VILI) preclinical ARDS models. Intravenous administration of eNAMPT-neutralizing antibodies, either a polyclonal (pAb) or a humanized monoclonal (mAb), significantly reduced the severity of murine acute inflammatory lung injury. Our study also confirms the critical role of endothelial cell (EC)-derived eNAMPT in ARDS pathobiology, extending previous reports of robust spatially-localized NAMPT expression in lung endothelium, epithelium, and resident and infiltrating leukocytes but without assessment of cell-specific NAMPT contributions to ARDS severity. Utilizing EC-specific conditional *NAMPT* KO mice, we now show the significant and unequivocal involvement of EC-secreted eNAMPT in dual preclinical ARDS models of injury. These studies strongly validate the viability of eNAMPT as an ARDS therapeutic target and underscore the capacity of an eNAMPT-neutralizing biologic therapy to directly address the unmet need for novel strategies that improve ARDS/VILI mortality.

MATERIALS AND METHODS

Reagents. Recombinant human eNAMPT was purchased from Peprotech (Cranbury, NJ). Antibodies that are immunoreactive against p-NFkB, pp-ERK, pp-p38, pp-JNK, IL-6, and IL-8 (KC) were purchased from Cell Signaling Technologies (Danvers, MA) and against β-actin from Invitrogen (Carlsbad, CA) (NFkB). Goat, rabbit, and mouse secondary antibodies were purchased from Life Technologies (Waltham, MA). IgG for use as controls was obtained from Jackson ImmuneResearch (West Grove, PA). Goat anti-human NAMPT pAb was custom-generated as previously described [17]. All other reagents were from Sigma-Aldrich (St. Louis, MO).

Generation of an eNAMPT-neutralizing humanized mAb. Two eNAMPT-neutralizing humanized mAbs, ALT-100 and ALT-300 were provided by Aqualung Therapeutics Corporation (Tucson, AZ) following *in vitro* mAb screening utilizing trans-EC electrical resistance assays [34, 35], NFkB activation biochemical assays [19] and *in vivo* screening utilizing dual preclinical ARDS models. ALT-100 was selected as the lead *in vivo* therapeutic and ALT-300 chosen for incorporation into the tissue NAMPT-imaging probe, ^{99m}Tc-ProNamptor^{TM}. Details of mAb generation and selection are supplied in Supplemental Materials and Methods.

^{99m}Tc-ProNamptor^{TM} mAb imaging. Extremely high NAMPT protein sequence homology exists between mice, rats, non-human primates, and humans (95-99%), underscoring ALT-100 and ALT-300 mAb utility in the murine preclinical studies we conducted including the ALT-300 mAb-containing fluorescent and ^{99m}Tc-labeled probes used for tissue imaging of NAMPT expression with human IgG serving as control [36, 37] (details of ALT-300 Cy5.5 or ^{99m}Tc labeling are available in Supplemental Materials and Methods). A mouse model of skin inflammation [38, 39] induced by topical

application of 12-O-tetradecanoylphorbol-13-acetate (TPA) was utilized to validate the ability of the Cy5.5-ALT-300 probe to detect NAMPT tissue expression *in vivo.* TPA was applied to the surface of the right ear, reapplied at 24h, and the left ear treated with acetone as the negative control. In separate experiments (n=3 mice), either Cy5.5-ALT-300 or Cy5.5-IgG (15-20 µg) was injected intravenously 3h after the second TPA/PBS application, followed by mouse imaging. To assess the capacity of the ^{99m}Tc-ALT-300 probe to detect *in vivo* NAMPT tissue expression, ^{99m}Tc-ProNamptor^{TM} (1.0-1.5 mCi, >98% radiochemical purity), [40, 41] or IgG control Ab was intravenously injected at 3h post LPS challenge in the "one-hit" model and imaged (Quantum Imaging Detector camera) [42-44]. Count activity-based measurements of ^{99m}Tc-ProNamptor^{TM} biodistribution and *ex vivo* autoradiography were performed in harvested lungs (see Supplemental Materials and Methods for additional details)**.**

Mouse strains. *In vivo* experiments utilized either wild type male C57BL/6J mice (8–12 weeks, Jackson Laboratories, Bar Harbor, ME), EC-specific conditional *NAMPT* knockout mice *(EC-cNAMPT$^{-/-}$)* on a mixed 129/B6 background, or littermate NAMPT$^{fl/fl}$ controls. *EC-cNAMPT$^{-/-}$* mice were generated by crossing floxed *NAMPT* mice (*NAMPT$^{fl/fl}$*) with tamoxifen-inducible EC-specific Cre transgenic mice (Tek-Cre/ERT2-1Soff) [45] with backcrossing with floxed homozygous *NAMPT* mice. After the final dose of tamoxifen, a two weeks minimal wait period was implemented before the utilization of *EC-cNAMPT$^{-/-}$* mice for experimentation (see Supplemental Materials and Methods for additional details)**.** EC-specific KO mice carrying the NAMPT flox transgene did not display discernible differences in phenotypic traits compared to their wild-type littermates. Growth rate, fecundity, and fertility also did not differ from wild-type mice.

Similarly, NAMPT flox mice crossed with the TIE2/ERT2 Cre mice to generate the conditional NAMPT KO line did not exhibit any phenotypic differences from either littermates or parental strains, both before and after tamoxifen injections.

eNAMPT-neutralizing strategies in "one-hit" and "two-hit" preclinical ARDS models. For the "one-hit" ARDS model, mice received an intratracheal LPS injection and were sacrificed at 18h post LPS as previously described [46-48]. For the "two-hit" LPS/VILI ARDS model, similar LPS-exposed mice were reintubated at 18h and placed on mechanical ventilation for 4h (tidal volume 20 ml/kg, respiratory rate 90 breaths/min, positive-end expiratory pressure 0 cm H_2O) as previously described [46-48]. In specific experiments, C57BL/6J mice received either the IV delivered eNAMPT-neutralizing pAb or the ALT-100 mAb (4mg/kg and 0.4mg/kg, respectively) or IgG control Ab (4mg/kg) (see Supplemental Materials and Methods for additional details)**.**

Bronchoalveolar lavage (BAL) analysis. BAL fluid retrieval, protein analysis, and cell count analysis including PMN determinations were performed as previously described [49] with additional details provided in the Supplemental Materials and Methods.

Evans Bue Dye extravasation assay. We evaluated lung vascular leakage by measuring extravascular Evans Blue Dye in the lung as we have rpeviousy described (58). Briefly, mice were injected Evans blue dye (0.05 mg, Sigma) i.v. 60 min before euthanasia. Lungs were then perfused to remove the intravascular dye, excised and homogenized in PBS. One volume of lung homogenate was incubated with 2 volumes of formamide and incubated at 60°C for 18 hrs before centrifugation. The optical density of the supernatant was measured at 620 nm and 740 nm using an Imark microplate

reader. Concentrations of Evans blue were corrected for the presence of heme pigments using the following formula: A_{620} (corrected) = A_{620} (raw)—(1.1927 X A_{720}) + 0.0071. The extravasated Evans blue dye concentrations were then calculated against a standard linear curve as a reflection of vascular protein leak into lung tissues.

Quantitative lung histology and immunohistochemistry (IHC) analyses. Hematoxylin and eosin staining: Lungs were fixed and sectioned for routine H & E staining and imaging (Olympus digital camera, 10x magnification) [50]. **NAMPT staining:** The avidin-biotin-peroxidase method was utilized with a rabbit anti-human NAMPT pAb (1:1000 dilution, Bethyl Laboratories, Montgomery, TX) for IHC visualization of NAMPT expression in lung tissues as previously described [14, 17, 19]. **NAMPT/β actin/CD-31 co-staining in *EC-cNAMPT*$^{-/-}$ mice**. Lung tissue sections from *EC-cNAMPT*$^{-/-}$ mice were incubated overnight (4^{o}C) with primary rabbit anti-human NAMPT pAb (Bethyl), β actin or rat anti-CD-31 mAb and stained with biotinylated secondary antibody (1h, 25^{o}C) and imaged (Zeiss Axiovert Photomicroscope, 10X objective, NA 0.4). **Quantitative analyses:** Histological and IHC images were randomly selected for H & E or NAMPT quantification using ImageJ software [51] with additional details provided in the Supplemental Materials and Methods.

Acute Lung Injury Severity Score (ALISS) quantification. The Acute Lung Injury Severity Score (ALISS) was utilized to integrate lung injury indices in the “one-hit” and “two-hit” preclinical ARDS models and to standardize the injury levels across the *in vivo* models. A ranking point system, incorporating published recommendations [59] objectively assigns a score to each study animal (1 to 4 points) for each of 4 severity of injury readouts (H & E histology quantification, BAL total protein concentration, BAL

total PMN cell count and plasma levels of the pro-inflammatory cytokine, IL-6). The maximal score for each animal is 16 points/mouse. In general, an ALISS score of 1-4 reflects the complete absence of injury, scores of 5-8 points reflect mild injury, scores of 9-12 points reflect moderate injury, and scores >12 points reflect severe injury. Additional details are provided in the Supplemental Materials and Methods.

Trans-endothelial electrical resistance (TER) measurements. Human pulmonary artery EC (Lonza, Walkersville, MD) were cultured as previously described [52] and seeded on evaporated gold microelectrodes (37°C, 5% CO_2) to measure TER using an electrical cell-substrate impedance sensing system (Applied Biophysics, Troy, NY) as previously described [53]. TER values from each microelectrode were pooled and plotted versus time (mean ± SEM).

Biochemical tissue and plasma levels of eNAMPT, NFkB, MAP kinases, IL-6, and IL-8. Western blotting of lung homogenates was performed according to standard protocols as previously reported [23, 49] with densitometric quantification of lung tissue expression of NAMPT, NFkB, MAP kinases, IL-6, and β-actin (total protein control). eNAMPT plasma levels were measured by ELISA as previously reported [27, 31], and plasma levels of IL-6 and IL-8 (KC) were measured utilizing a meso-scale ELISA platform (Meso Scale Diagnostics, Rockville, MD) (described in **Supplemental Materials and Methods).**

Statistical analysis. Continuous data were compared using nonparametric methods and categorical data by the chi-square test. Where applicable, standard one-way ANOVA was used, and groups were compared using the Newman-Keuls test. Two-way ANOVA was used to compare the means of data from two or more different

experimental groups. If a significant difference was present by ANOVA ($p < 0.05$), the least significant differences (LSD) test was performed post hoc. Statistical tests were performed using GraphPad Prism version 7.00 for Windows, GraphPad Software, La Jolla California USA, www.graphpad.com. Statistical significance was considered at $p < 0.05$.

RESULTS

Increased lung tissue NAMPT expression in preclinical murine ARDS models. Compared to control mice, IHC lung tissue staining from mice exposed to either the "one-hit" (LPS 18h) ARDS model **(Figure 1A)** or the "two-hit" (LPS 18h, ventilation 4h) ARDS/VILI model (**Figure 1C)** demonstrated dramatic upregulation of NAMPT expression (alveolar epithelium, endothelium, macrophages, neutrophils) summarized in **Figures 1B/1D** ($p<0.05$) and confirmed in lung homogenates from LPS-challenged mice. NAMPT protein expression was significantly elevated beginning 2h post LPS challenge, peaking at 4h, and returning towards baseline by 18h **(Figure 1E).**

***In vivo* detection of NAMPT lung tissue expression.** Validation of the ProNamptor^{TM} mAb probe for detection of tissue inflammation was observed with the TPA-induced ear inflammation model with a significantly higher accumulation of Cy5.5-ProNamptor^{TM} observed relative to the control Cy5.5-IgG (*in vivo* fluorescence imaging post-injection) **(Figure 2A).** In both unchallenged control mice and LPS-challenged mice exposed to injected either the ^{9m}Tc-IgG control or ^{99m}Tc-ProNamptor^{TM}, there was prominent accumulation of radioactivity in the liver and in the cardiac blood pool and, to much lesser extent, in the lung **(Figure 2B).** However, *in vivo* and *ex vivo* imaging

demonstrated significantly increased radioactive accumulation of ^{99m}Tc-ProNamptor^{TM} in lung tissues from mice exposed to the “one-hit” LPS ARDS model (imaged at 7h, **Figure 2B)** confirmed by *ex vivo* autoradiograph images **(Figure 2C).** Quantification of ^{99m}Tc uptake in lung tissues at 7hrs post LPS challenge showed significant increases in both the non-specific IgG as well as ProNamptor^{TM}, however, the magnitude of ^{99m}Tc-ProNamptor^{TM} radioactivity uptake was significantly increased compared to IgG control and unchallenged mice **(Figure 2C/D)**. The marked increase in ^{99m}Tc-ProNamptor^{TM} radiolabel uptake at 7h post LPS waned substantially by 10h post LPS challenge **(Figure 2D/E)**, a finding that is consistent with levels of NAMPT protein expression in lung tissue homogenates depicted in **Figure 1E**.

eNAMPT-neutralizing strategies attenuate “one-hit” preclinical ARDS injury. H&E lung tissue staining from the “one-hit” LPS-challenged ARDS model show alveolar inflammation with significant neutrophil infiltration and alveolar edema compared to control mice (inset) **(Figure 3A)**. Intravenous administration of either the eNAMPT-neutralizing pAb (4 mg/kg) or the ALT-100 mAb (0.4 mg/kg) significantly reduced histologic injury **(Figure 3A)**, which was verified by the significant reductions in LPS-induced inflammatory indices i.e. BAL protein **(Figure 3C)** and PMN counts **(Figure 3D)**. The lung protection afforded by ALT-100 mAb was significantly superior to the eNAMPT pAb as reflected either by H&E staining **(Figure 3B)** or as captured in the integrated acute lung injury severity score or ALISS (H&E staining, BAL protein, BAL PMN counts, plasma IL-6 concentration) **(Figure 3E)**.

eNAMPT-neutralizing strategies attenuate “two-hit” ARDS/VILI injury. H&E staining in mice exposed to the “two-hit” ARDS/VILI model (LPS exposure 22h,

ventilator exposure for the final 4h) revealed significant inflammatory cell infiltration into the lung parenchyma accompanied by both interstitial and alveolar edema when compared to control mice (inset) **(Figure 4A)**. As with the “one-hit” LPS model, the severity of histologic injury in the “two-hit” LPS/VILI model was significantly reduced by i.v. delivery of either the eNAMPT-neutralizing pAb (4 mg/kg) or the ALT-100 mAb (0.4 mg/kg) **(Figure 4A/B)**. Both eNAMPT-neutralizing biologic strategies also significantly reduced BAL protein (**Figure 4C)** and BAL PMN counts **(Figure 4D)** with greater ALT-100 mAb-mediated protection compared with the polyclonal Ab **(Figure 4E)**.

The eNAMPT neutralization attenuates LPS- and LPS/VILI-challenged human lung EC signaling and barrier responses *in vitro* and *in vivo*. We previously demonstrated that NAMPT expression in a preclinical VILI model is primarily spatially-localized to lung EC, lung epithelium, and to resident and infiltrating leukocytes [13, 14]. We sought to specifically characterize lung endothelium as a target tissue for circulating eNAMPT and to assess the contribution of lung EC-derived NAMPT to the severity of acute lung injury in preclinical models of ARDS/VILI. Initial *in vitro* experiments utilizing human lung EC confirmed that eNAMPT ligation of TLR4 induces robust NFkB phosphorylation [19] and MAP kinase activation (p38, JNK, p42/44 ERK) with these signaling responses nearly abolished by the eNAMPT neutralizing pAb (**Figure 5A/5B**) as were eNAMPT-induced declines in trans-human lung EC electrical resistance (TER), reflecting pAb- and mAb-mediated protection against eNAMPT-induced loss of EC barrier integrity (**Figure 5C/5D).** The ALT-100 mAb, but not the eNAMPT-neutralizing pAb, also produced significant reductions in LPS-induced barrier disruption **(Figure 5D)**,

results consistent with the contributory role of LPS-mediated eNAMPT secretion (maximal at 4 h, **Figure 1E)** in loss of EC barrier integrity and reductions in TER.

The contribution of circulating eNAMPT to the loss of lung vascular barrier integrity was next examined *in vivo* initially with the Evan's blue dye accumulation in lung tissues, an index of vascular permeability, which demonstrated dramatic ALT-100 mAb-mediated restoration of EC barrier integrity in the "one-hit" (LPS) preclinical ARDS model **(Figure 5E)**. To validate our *in vitro* findings that specifically characterized increased MAP kinase signaling in eNAMPT-challenged lung endothelium, we examined levels of MAP kinase pathway signaling in lung tissues from mice exposed to both "one-hit" and "two-hit" preclinical ARDS models. **Figure 6** demonstrates the activation of NFkB and MAP kinase family effectors (p38, JNK, p42/44 ERK), reflected by phosphorylation in lung tissue homogenates [19], in both preclinical ARDS models. Importantly, the ALT-100 mAb effectively suppressed the robust NFkB and MAP kinase family activation observed in the two ARDS models consistent with the contribution of circulating eNAMPT to the severity of lung injury in preclinical models of ARDS/VILI (**Figure 6**).

EC-specific *NAMPT* deletion *in vivo* reduces "one-hit" and "two-hit" lung injury. We utilized genetically-engineered conditional *EC-cNAMPT*$^{-/-}$ KO mice, with conditional *NAMPT* deletion restricted to EC, to further explore the contribution of lung EC-specific expression and secretion of NAMPT to the development of "one-hit" and "two-hit" lung injury. Lung tissue IHC studies demonstrated that tamoxifen-treated *EC-cNAMPT*$^{-/-}$ KO mice exhibit selective loss of NAMPT staining in lung endothelium whereas lung epithelial NAMPT expression was robust (**Figure 7A**), reflecting

conditional deletion of NAMPT expression in lung EC (compared to wild type mice). Examination of H&E lung tissue staining in “one-hit” or “two-hit”-exposed *EC-cNAMPT*$^{-/-}$ KO mice showed significant reductions in inflammatory lung tissue injury (**Figure 7B-D**), accompanied by reduced BAL protein levels (**Figure 7E**) and BAL PMN counts (**Figure 7F**) compared to similarly exposed littermate control mice. The significant protection afforded by EC-specific *NAMPT* deletion in *EC-cNAMPT*$^{-/-}$ mice was captured in the integrated lung injury severity score (ALISS, **Figure 7G)**.

Lastly, we explored the involvement of EC-derived circulating eNAMPT to the severity of acute lung injury and measured eNAMPT plasma levels in “one-hit”- and “two-hit”-exposed *EC-cNAMPT*$^{-/-}$ and littermate control mice. Compared to littermate controls, both “one-hit”- and “two-hit”-exposed *EC-cNAMPT*$^{-/-}$ mice demonstrated reduced plasma eNAMPT levels (**Figures 8A**) as well as reduced plasma levels of IL-6 and IL-8 (KC in mice), two inflammatory cytokines often implicated as components in the ARDS “cytokine storm” **(Figure 8B/C).** Plasma levels of both IL-6 and IL-8 (KC) in “one-hit”- and “two-hit”-exposed WT C57Bl6 mice were also significantly reduced in ALT-100 mAb-treated mice compared to untreated mice **(Figure 8D),** validated by the decreased IL-6 protein expression in “two-hit” ARDS-exposed mice treated with the eNAMPT-neutralizing ALT-100 mAb **(Figure 8F).**

DISCUSSION

Currently, there are no FDA-approved ARDS therapies, a serious unmet need that's has been dramatically highlighted by the current COVID-19 pandemic. To potentially address the need for pharmacotherapies that reduce ARDS mortality, we previously

identified eNAMPT, a novel DAMP [19], as a potentially attractive ARDS target whose expression and function tightly link to human ARDS. For example, NAMPT expression is highly induced by ARDS-relevant stimuli such as bacterial infection, hypoxia, shock, trauma and excessive mechanical stress produced by mechanical ventilation [20-23]. Further, plasma levels of eNAMPT are a biomarker for ARDS severity [14, 17, 22, 29-31, 33], and *NAMPT* genotypes with elevated minor allelic frequencies (i.e., common SNPs) confer a significant risk of increased ARDS severity and mortality in both Blacks and non-Hispanic whites [14, 17, 22, 29-31, 33]. Our earlier studies strongly implicated an essential contribution of eNAMPT to both VILI and ARDS pathobiology [14, 17, 22, 29-31, 33] via upstream activation of inflammatory cascades as a consequence of TLR4 ligation and NFkB transcriptional activities [19]. Thus, there is a substantial and compelling foundational basis for eNAMPT as a viable therapeutic target in ARDS/VILI.

Our current study underscores eNAMPT involvement in ARDS pathobiology in several important and novel ways. First, we utilized complementary approaches to validate increased NAMPT lung tissue expression in both “one-hit” (LPS) and “two-hit” (LPS/VILI) preclinical ARDS models. IHC and biochemical studies revealed markedly increased NAMPT lung tissue expression in both preclinical models. This was further verified utilizing the radiolabeled probe, ^{99m}Tc-ProNamptor^{TM}, with temporally increased LPS-induced NAMPT lung tissue expression that aligned with NAMPT expression in lung homogenates. As ^{99m}Tc-ProNamptor^{TM} contains the radiolabeled eNAMPT-neutralizing mAb (ALT-300), the potential exists for ^{99m}Tc-ProNamptor^{TM} to serve as a novel molecular imaging theranostic that may therapeutically reduce inflammatory injury, a hypothesis to be addressed in future studies.

A second significant implication of this work is to extend our earlier studies in VILI murine models and directly explore eNAMPT-neutralization as an effective ARDS therapy. Previous intratracheal instillation of an eNAMPT-neutralizing polyclonal pAb supported eNAMPT as a relevant VILI therapeutic target [17, 19]. We now extend this work to demonstrate intravenous administration of ALT-100, the eNAMPT-neutralizing humanized mAb, significantly reduced the severity of inflammatory lung injury in both preclinical ARDS models and was significantly more protective than the eNAMPT pAb**.** Our use of dual preclinical ARDS models adds significant rigor to our work and directly addresses suggestions that a major failure of ARDS pharmacologic interventions is due to use of a single preclinical ARDS murine model [54, 55].

Our preclinical results support our nascent ARDS clinical trial strategy which is designed to deliver the ALT-100 mAb to ARDS subjects with respiratory failure at the time of intubation i.e. prior to initiation of mechanical ventilation. This trial design specifically targets VILI prevention and the dampening of ventilator-induced amplification of inflammatory pathways to reduce multi-organ injury, thereby minimizing the duration of mechanical ventilation, improving ICU survival, and reducing healthcare costs. Prior unsuccessful ARDS therapeutic clinical trials, primarily targeting single cytokines or bacterial products, were likely hampered by delays in targeted therapy delivery [56, 57], with initiation of therapy well after the onset of amplified innate immunity-driven lung and systemic inflammatory pathways. The feasibility of administering ALT-100 to ARDS subjects with impending respiratory failure in the ER or upon entry to the ICU, prior to intubation and exposure to mechanical ventilation, was previously a daunting challenge from a clinical trial perspective, but is supported by

recent ER-ICU clinical trials.

Another valuable insight provided by our study is to underscore the critical importance of EC-derived circulating eNAMPT to ARDS pathobiology [14, 35]. While NAMPT expression, in addition to lung ECs, is robust in lung alveolar epithelium and in resident and infiltrating leukocytes in VILI-challenged canine and murine models [13, 14], the critical contribution of each cellular component to ARDS severity was previously unknown. Our current *in vitro* and in vivo studies confirm earlier work that highlighted lung EC as a key eNAMPT cellular target with dysregulation of lung EC permeability responses [35]. We now show potent eNAMPT-mediated activation of human lung EC TLR4 and MAP kinase pathways and loss of EC barrier integrity, responses strongly abrogated by both eNAMPT-neutralizing modalities (pAb, ALT-100 mAb). The modest but significant inhibition of LPS-induced declines in trans EC electrical resistance barrier dysfunction by ALT-100 mAb is again consistent with the contribution of eNAMPT, secreted by EC in response to LPS, to increased vascular permeability, supported by the profound reductions in Evans blue dye acculumulation **(Figure 5E)** and dramatic reductions in MAP kinase signaling in vivo **(Figure 6)**. To directly interrogate the role of EC-derived eNAMPT *in vivo*, we utilized an *EC-cNAMPT*$^{-/-}$ mouse line with targeted KO of eNAMPT that is conditionally restricted to the endothelium. *EC-cNAMPT*$^{-/-}$ mice were significantly protected in both “one-hit” and “two-hit” preclinical ARDS injury models and exhibited significantly reduced plasma levels of eNAMPT, IL-6, and IL-8 (KC) when compared to WT littermates. These results mirror the reductions in plasma and tissue levels of IL-6 in ALT-100-treated mice exposed to “one-hit” and “two-hit” ARDS models

indicating that EC-derived circulating eNAMPT is likely a significant contributor to ARDS pathobiology.

In summary, our studies strongly validate targeting of the eNAMPT/TLR4 inflammatory pathway with a humanized eNAMPT-neutralizing mAb as a viable therapeutic strategy to address the serious unmet need for effective and specific pharmacologic therapies to improve ARDS/VILI mortality. We have also clarified the essential and contributory role of EC-derived eNAMPT to inflammatory lung injury elicited by bacterial infection and by ventilator-induced mechanical stress. Finally, it is well known that the vast heterogeneity of ARDS has been a critical challenge to the conduct of successful therapeutic clinical trials in the U.S. and by ARDS clinical trial networks world-wide. Our study demonstrates that with the combined availability of i) eNAMPT as an ARDS predictive plasma biomarker, either alone [14, 32, 33], or as part of an ARDS biomarker panel [31]; ii) identification of high-risk *NAMPT* genotypes [14, 29, 30]; and iii) a highly efficacious eNAMPT-neutralizing humanized mAb as targeted biologic therapy, the opportunity exists for novel ARDS clinical trial designs for that stratify patient enrollment for testing a biologic therapy that targets the eNAMPT/TLR4 inflammatory pathway, an attractive mechanism to deliver personalized ICU medicine in the current COVID-19 pandemic landscape.

REFERENCES

1. Gong T, Liu L, Jiang W, Zhou R. DAMP-sensing receptors in sterile inflammation and inflammatory diseases. *Nat Rev Immunol* 2020: 20(2): 95-112.

2. Kono H, Rock KL. How dying cells alert the immune system to danger. *Nat Rev Immunol* 2008: 8(4): 279-289.
3. Mathew G, Unnikrishnan MK. Multi-target drugs to address multiple checkpoints in complex inflammatory pathologies: evolutionary cues for novel "first-in-class" anti-inflammatory drug candidates: a reviewer's perspective. *Inflamm Res* 2015: 64(10): 747-752.
4. Denning NL, Aziz M, Gurien SD, Wang P. DAMPs, and NETs in Sepsis. *Front Immunol* 2019: 10: 2536.
5. Matthay MA, Zimmerman GA, Esmon C, Bhattacharya J, Coller B, Doerschuk CM, Floros J, Gimbrone MA, Jr., Hoffman E, Hubmayr RD, Leppert M, Matalon S, Munford R, Parsons P, Slutsky AS, Tracey KJ, Ward P, Gail DB, Harabin AL. Future research directions in acute lung injury: summary of a National Heart, Lung, and Blood Institute working group. *Am J Respir Crit Care Med* 2003: 167(7): 1027-1035.
6. Singer M, Deutschman CS, Seymour CW, Shankar-Hari M, Annane D, Bauer M, Bellomo R, Bernard GR, Chiche JD, Coopersmith CM, Hotchkiss RS, Levy MM, Marshall JC, Martin GS, Opal SM, Rubenfeld GD, van der Poll T, Vincent JL, Angus DC. The Third International Consensus Definitions for Sepsis and Septic Shock (Sepsis-3). *JAMA : the journal of the American Medical Association* 2016: 315(8): 801-810.
7. Ware LB, Matthay MA. The acute respiratory distress syndrome. *N Engl J Med* 2000: 342(18): 1334-1349.
8. Rubenfeld GD, Caldwell E, Peabody E, Weaver J, Martin DP, Neff M, Stern EJ, Hudson LD. Incidence and outcomes of acute lung injury. *N Engl J Med* 2005: 353(16): 1685-1693.
9. Rubenfeld GD, Herridge MS. Epidemiology and outcomes of acute lung injury. *Chest* 2007: 131(2): 554-562.
10. Zambon M, Vincent JL. Mortality rates for patients with acute lung injury/ARDS have decreased over time. *Chest* 2008: 133(5): 1120-1127.
11. Rubartelli A, Lotze MT. Inside, outside, upside down: damage-associated molecular-pattern molecules (DAMPs) and redox. *Trends Immunol* 2007: 28(10): 429-436.
12. Grigoryev DN, Ma SF, Irizarry RA, Ye SQ, Quackenbush J, Garcia JG. Orthologous gene-expression profiling in multi-species models: search for candidate genes. *Genome biology* 2004: 5(5): R34.
13. Simon BA, Easley RB, Grigoryev DN, Ma SF, Ye SQ, Lavoie T, Tuder RM, Garcia JG. Microarray analysis of regional cellular responses to local mechanical stress in acute lung injury. *American journal of physiology* 2006: 291(5): L851-861.
14. Ye SQ, Simon BA, Maloney JP, Zambelli-Weiner A, Gao L, Grant A, Easley RB, McVerry BJ, Tuder RM, Standiford T, Brower RG, Barnes KC, Garcia JG. Pre-B-cell colony-enhancing factor as a potential novel biomarker in acute lung injury. *Am J Respir Crit Care Med* 2005: 171(4): 361-370.
15. Mitra S, Wade MS, Sun X, Moldobaeva N, Flores C, Ma SF, Zhang W, Garcia JG, Jacobson JR. GADD45a promoter regulation by a functional genetic variant associated with acute lung injury. *PloS one* 2014: 9(6): e100169.
16. Meyer NJ, Huang Y, Singleton PA, Sammani S, Moitra J, Evenoski CL, Husain AN, Mitra S, Moreno-Vinasco L, Jacobson JR, Lussier YA, Garcia JG. GADD45a is a novel candidate gene in inflammatory lung injury via influences on Akt signaling. *FASEB journal : official publication of the Federation of American Societies for Experimental Biology* 2009: 23(5): 1325-1337.
17. Hong SB, Huang Y, Moreno-Vinasco L, Sammani S, Moitra J, Barnard JW, Ma SF, Mirzapoiazova T, Evenoski C, Reeves RR, Chiang ET, Lang GD, Husain AN, Dudek SM, Jacobson JR, Ye SQ, Lussier YA, Garcia JG. Essential role of pre-B-cell colony enhancing factor in ventilator-induced lung injury. *Am J Respir Crit Care Med* 2008: 178(6): 605-617.
18. Gao L, Flores C, Fan-Ma S, Miller EJ, Moitra J, Moreno L, Wadgaonkar R, Simon B, Brower R, Sevransky J, Tuder RM, Maloney JP, Moss M, Shanholtz C, Yates CR, Meduri GU,

Ye SQ, Barnes KC, Garcia JG. Macrophage migration inhibitory factor in acute lung injury: expression, biomarker, and associations. *Transl Res* 2007: 150(1): 18-29.
19. Camp SM, Ceco E, Evenoski CL, Danilov SM, Zhou T, Chiang ET, Moreno-Vinasco L, Mapes B, Zhao J, Gursoy G, Brown ME, Adyshev DM, Siddiqui SS, Quijada H, Sammani S, Letsiou E, Saadat L, Yousef M, Wang T, Liang J, Garcia JG. Unique Toll-Like Receptor 4 Activation by NAMPT/PBEF Induces NFkappaB Signaling and Inflammatory Lung Injury. *Sci Rep* 2015: 5: 13135.
20. Adyshev DM, Elangovan VR, Moldobaeva N, Mapes B, Sun X, Garcia JG. Mechanical stress induces pre-B-cell colony-enhancing factor/NAMPT expression via epigenetic regulation by miR-374a and miR-568 in human lung endothelium. *American journal of respiratory cell and molecular biology* 2014: 50(2): 409-418.
21. Elangovan VR, Camp SM, Kelly GT, Desai AA, Adyshev D, Sun X, Black SM, Wang T, Garcia JG. Endotoxin- and mechanical stress-induced epigenetic changes in the regulation of the nicotinamide phosphoribosyltransferase promoter. *Pulm Circ* 2016: 6(4): 539-544.
22. Sun X, Elangovan VR, Mapes B, Camp SM, Sammani S, Saadat L, Ceco E, Ma SF, Flores C, MacDougall MS, Quijada H, Liu B, Kempf CL, Wang T, Chiang ET, Garcia JG. The NAMPT promoter is regulated by mechanical stress, signal transducer and activator of transcription 5, and acute respiratory distress syndrome-associated genetic variants. *American journal of respiratory cell and molecular biology* 2014: 51(5): 660-667.
23. Sun X, Sun BL, Babicheva A, Vandenpool R, Oita RC, Casanova N, Tang H, Gupta A, Lynn H, Gupta G, Rischard F, Sammani S, Kempf CL, Moreno-Vinasco L, Ahmed M, Camp SM, Wang J, Desai AA, Yuan JX, Garcia JG. Direct eNAMPT involvement in pulmonary hypertension and vascular remodeling: Transcriptional regulation by SOX and HIF2α. *American journal of respiratory cell and molecular biology* 2020: In press.
24. Revollo JR, Grimm AA, Imai S. The regulation of nicotinamide adenine dinucleotide biosynthesis by Nampt/PBEF/visfatin in mammals. *Current opinion in gastroenterology* 2007: 23(2): 164-170.
25. Revollo JR, Korner A, Mills KF, Satoh A, Wang T, Garten A, Dasgupta B, Sasaki Y, Wolberger C, Townsend RR, Milbrandt J, Kiess W, Imai S. Nampt/PBEF/Visfatin regulates insulin secretion in beta cells as a systemic NAD biosynthetic enzyme. *Cell metabolism* 2007: 6(5): 363-375.
26. Moreno-Vinasco L, Quijada H, Sammani S, Siegler J, Letsiou E, Deaton R, Saadat L, Zaidi RS, Messana J, Gann PH, Machado RF, Ma W, Camp SM, Wang T, Garcia JG. Nicotinamide phosphoribosyltransferase inhibitor is a novel therapeutic candidate in murine models of inflammatory lung injury. *American journal of respiratory cell and molecular biology* 2014: 51(2): 223-228.
27. Oita RC, Camp SM, Ma W, Ceco E, Harbeck M, Singleton P, Messana J, Sun X, Wang T, Garcia JGN. Novel Mechanism for Nicotinamide Phosphoribosyltransferase Inhibition of TNF-alpha-mediated Apoptosis in Human Lung Endothelial Cells. *American journal of respiratory cell and molecular biology* 2018: 59(1): 36-44.
28. Bajwa EK, Boyce PD, Januzzi JL, Gong MN, Thompson BT, Christiani DC. Biomarker evidence of myocardial cell injury is associated with mortality in acute respiratory distress syndrome. *Critical care medicine* 2007: 35(11): 2484-2490.
29. Bajwa EK, Yu CL, Gong MN, Thompson BT, Christiani DC. Pre-B-cell colony-enhancing factor gene polymorphisms and risk of acute respiratory distress syndrome. *Crit Care Med* 2007: 35(5): 1290-1295.
30. O'Mahony DS, Glavan BJ, Holden TD, Fong C, Black RA, Rona G, Tejera P, Christiani DC, Wurfel MM. Inflammation and immune-related candidate gene associations with acute lung injury susceptibility and severity: a validation study. *PloS one* 2012: 7(12): e51104.

31. Bime C, Casanova N, Oita RC, Ndukum J, Lynn H, Camp SM, Lussier Y, Abraham I, Carter D, Miller EJ, Mekontso-Dessap A, Downs CA, Garcia JGN. Development of a biomarker mortality risk model in acute respiratory distress syndrome. *Crit Care* 2019: 23(1): 410.
32. Lee K, Huh JW, Lim CM, Koh Y, Hong SB. Clinical role of serum pre-B cell colony-enhancing factor in ventilated patients with sepsis and acute respiratory distress syndrome. *Scandinavian journal of infectious diseases* 2013: 45(10): 760-765.
33. Lee KA, Gong MN. Pre-B-cell colony-enhancing factor and its clinical correlates with acute lung injury and sepsis. *Chest* 2011: 140(2): 382-390.
34. Garcia JG, Schaphorst KL, Verin AD, Vepa S, Patterson CE, Natarajan V. Diperoxovanadate alters endothelial cell focal contacts and barrier function: role of tyrosine phosphorylation. *J Appl Physiol (1985)* 2000: 89(6): 2333-2343.
35. Ye SQ, Zhang LQ, Adyshev D, Usatyuk PV, Garcia AN, Lavoie TL, Verin AD, Natarajan V, Garcia JG. Pre-B-cell-colony-enhancing factor is critically involved in thrombin-induced lung endothelial cell barrier dysregulation. *Microvasc Res* 2005: 70(3): 142-151.
36. Klohs J, Grafe M, Graf K, Steinbrink J, Dietrich T, Stibenz D, Bahmani P, Kronenberg G, Harms C, Endres M, Lindauer U, Greger K, Stelzer EH, Dirnagl U, Wunder A. In vivo imaging of the inflammatory receptor CD40 after cerebral ischemia using a fluorescent antibody. *Stroke* 2008: 39(10): 2845-2852.
37. Zhang Q, Wang F, Wu YS, Zhang KK, Lin Y, Zhu XQ, Lv JQ, Lu XS, Zhang XL, Hu Y, Huang YP. Dual-color labeled anti-mucin 1 antibody for imaging of ovarian cancer: A preliminary animal study. *Oncol Lett* 2015: 9(3): 1231-1235.
38. Kim EJ, Park H, Kim J, Park JH. 3,3'-diindolylmethane suppresses 12-O-tetradecanoylphorbol-13-acetate-induced inflammation and tumor promotion in mouse skin via the downregulation of inflammatory mediators. *Mol Carcinog* 2010: 49(7): 672-683.
39. Liu Z, Wyffels L, Barber C, Wan L, Xu H, Hui MM, Furenlid LR, Woolfenden JM. Characterization of 99mTc-labeled cytokine ligands for inflammation imaging via TNF and IL-1 pathways. *Nucl Med Biol* 2012: 39(7): 905-915.
40. Malviya G, D'Alessandria C, Bonanno E, Vexler V, Massari R, Trotta C, Scopinaro F, Dierckx R, Signore A. Radiolabeled humanized anti-CD3 monoclonal antibody visilizumab for imaging human T-lymphocytes. *J Nucl Med* 2009: 50(10): 1683-1691.
41. Ouadi A, Bekaert V, Receveur N, Thomas L, Lanza F, Marchand P, Gachet C, Mangin PH, Brasse D, Laquerriere P. Imaging thrombosis with (99m)Tc-labeled RAM.1-antibody in vivo. *Nucl Med Biol* 2018: 61: 21-27.
42. Miller BW, Gregory SJ, Fuller ES, Barrett HH, Barber HB, Furenlid LR. The iQID camera: An ionizing-radiation quantum imaging detector. *Nucl Instrum Methods Phys Res A* 2014: 767: 146-152.
43. Furenlid LR, Barrett HH, Barber HB, Clarkson EW, Kupinski MA, Liu Z, Stevenson GD, Woolfenden JM. Molecular Imaging in the College of Optical Sciences - An Overview of Two Decades of Instrumentation Development. *Proc SPIE Int Soc Opt Eng* 2014: 9186.
44. Han L, Miller BW, Barber HB, Nagarkar VV, Furenlid LR. A New Columnar CsI(Tl) Scintillator for iQID detectors. *Proc SPIE Int Soc Opt Eng* 2014: 9214: 92140D.
45. Korhonen H, Fisslthaler B, Moers A, Wirth A, Habermehl D, Wieland T, Schutz G, Wettschureck N, Fleming I, Offermanns S. Anaphylactic shock depends on endothelial Gq/G11. *J Exp Med* 2009: 206(2): 411-420.
46. Goldman JL, Sammani S, Kempf C, Saadat L, Letsiou E, Wang T, Moreno-Vinasco L, Rizzo AN, Fortman JD, Garcia JG. Pleiotropic effects of interleukin-6 in a "two-hit" murine model of acute respiratory distress syndrome. *Pulm Circ* 2014: 4(2): 280-288.
47. Letsiou E, Rizzo AN, Sammani S, Naureckas P, Jacobson JR, Garcia JG, Dudek SM. Differential and opposing effects of imatinib on LPS- and ventilator-induced lung injury. *American journal of physiology* 2015: 308(3): L259-269.

48. Rizzo AN, Sammani S, Esquinca AE, Jacobson JR, Garcia JG, Letsiou E, Dudek SM. Imatinib attenuates inflammation and vascular leak in a clinically relevant two-hit model of acute lung injury. *American journal of physiology* 2015: 309(11): L1294-1304.
49. Peng X, Hassoun PM, Sammani S, McVerry BJ, Burne MJ, Rabb H, Pearse D, Tuder RM, Garcia JG. Protective effects of sphingosine 1-phosphate in murine endotoxin-induced inflammatory lung injury. *Am J Respir Crit Care Med* 2004: 169(11): 1245-1251.
50. Geraci-Erck M. Immunohistochemistry Research Applications for Animal Tissue. *NSH 32nd Symposium*: Wokshop #82: 1-67.
51. Jensen EC. Quantitative analysis of histological staining and fluorescence using ImageJ. *Anat Rec (Hoboken)* 2013: 296(3): 378-381.
52. Dudek SM, Jacobson JR, Chiang ET, Birukov KG, Wang P, Zhan X, Garcia JG. Pulmonary endothelial cell barrier enhancement by sphingosine 1-phosphate: roles for cortactin and myosin light chain kinase. *The Journal of biological chemistry* 2004: 279 23): 24692-24700.
53. Garcia JG, Liu F, Verin AD, Birukova A, Dechert MA, Gerthoffer WT, Bamberg JR, English D. Sphingosine 1-phosphate promotes endothelial cell barrier integrity by Edg-dependent cytoskeletal rearrangement. *The Journal of clinical investigation* 2001: 108 5): 689-701.
54. Jagrosse ML, Dean DA, Rahman A, Nilsson BL. RNAi therapeutic strategies for acute respiratory distress syndrome. *Transl Res* 2019: 214: 30-49.
55. Oakley C, Koh M, Baldi R, Soni S, O'Dea K, Takata M, Wilson M. Ventilation following established ARDS: a preclinical model framework to improve predictive power. *Thorax* 2019: 74(12): 1120-1129.
56. Fuller BM, Mohr NM, Hotchkiss RS, Kollef MH. Reducing the burden of acute respiratory distress syndrome: the case for early intervention and the potential role of the emergency department. *Shock* 2014: 41(5): 378-387.
57. Malaviya R, Laskin JD, Laskin DL. Anti-TNFalpha therapy in inflammatory lung diseases. *Pharmacol Ther* 2017: 180: 90-98.
58. Moitra J, Sammani S, Garcia JG. Re-evaluation of Evans Blue dye as a marker of albumin clearance in murine models of acute lung injury. *Transl Res*. 2007: 150(4):253-65.
59. Matute-Bello G, Downey G, Moore BB, Groshong SD, Matthay MA, Slutsky AS, Kuebler WM, Acute Lung Injury in Animals Study Group. An official American Thoracic Society workshop report: features and measurements of experimental acute lung injury in animals. *Am J Respir Cell Mol Biol* 2011: 44(5):725-38.

FIGURE LEGENDS

Figure 1. Increased NAMPT expression in lung tissues from "one-hit" and "two-hit" preclinical ARDS murine models. IHC staining to visualize NAMPT expression in lung tissues utilized a rabbit anti-human mAb (Bethyl, Montgomery TX). Compared to control, unchallenged C57BL/6J mice, marked increases in NAMPT expression were observed in lung tissues from mice exposed to either a "one-hit" LPS ARDS model (intratracheal LPS, 18h) (**Panel A**) or a "two-hit" preclinical ARDS/VILI model (LPS 22h, ventilator exposure for final 4h, tidal volume 20 mL/kg) (**Panel C**). NAMPT expression was most prominent in alveolar epithelium, endothelium, macrophages, and infiltrating neutrophils (insets). Changes in NAMPT IHC staining were quantitatively summarized (**Panels B/D,** Image J software) (n >5/group, *p<0.05 for LPS or LPS/VILI vs. control). We also assessed NAMPT protein expression in lung homogenates (Western blotting) at various times post LPS challenge (**Panel E**). Densitometric analysis (n=4 each time point) showed significant time-dependent increases in NAMPT immunoreactivity, peaking at 4h post LPS (*p< 0.05).

Figure 2. ProNamptor^{TM} detects NAMPT expression *in vivo* in the "one-hit" LPS preclinical ARDS model. A. To validate the eNAMPT-specific mAb-containing ProNamptor^{TM} probe's capacity to detect inflammatory injury, studies were conducted in the TPA-induced inflammatory ear model. Representative fluorescence images of Cy5.5-IgG (left) and the eNAMPT-specific imaging probe, Cy5.5-ProNamptor^{TM} (right), acquired 12h after probe injection in two TPA-injected mice with right ear edema.

Significantly enhanced fluorescence accumulation was observed in the inflamed right ear of a mouse injected with Cy5.5-ProNamptor^{TM} compared to the Cy5.5-IgG-imaged mouse (arrows). **B.** Representative whole-body iQID images in an unchallenged control mouse and in LPS-challenged C57BL/6J mice injected with either a non-specific ^{99m}Tc-IgG Ab probe or with ^{99m}Tc-ProNamptor^{TM}. Images were collected 7h post LPS instillation (3h post ^{99m}Tc-ProNamptor^{TM} injection). Magnified thoracic images highlight the detection of NAMPT expression in LPS-induced lung inflammation. Increased radioactivity is noted for both the non-specific ^{99m}Tc-IgG Ab and the ^{99m}Tc-ProNamptor^{TM} probes in the liver and the cardiac blood pool (outlined in red) of LPS-challenged animals. However increased lung accumulation was observed with the ^{99m}Tc-ProNamptor^{TM} (chest area marked by white dashes), **C.** Significantly higher radioactive accumulation of ^{99m}Tc-ProNamptor^{TM} in LPS-injured lungs (7h, compared to IgG Ab-^{99m}Tc and to control lungs) was further confirmed by *ex vivo* lung autoradiograph imaging (representative image, n=4). **D/E.** *In vivo* quantitative image analysis and *ex vivo* biodistribution measurements (%ID/g) demonstrate significant increased ^{99m}Tc-ProNamptor^{TM} pulmonary uptake in LPS-injured lungs at 7h post LPS with waning of NAMPT uptake/expression by 10h compared to ^{99m}Tc-IgG Ab and control lungs (*$p<0.01$ compared to controls).

Figure 3. eNAMPT-neutralizing strategies attenuate "one-hit" preclinical ARDS injury. A. H&E lung tissue staining from mice exposed to the "one-hit" LPS/ARDS injury model (18h, **left**) show interstitial and alveolar inflammation with significant neutrophil infiltration and alveolar edema compared to control C57BL/6J mice (inset). The severity of LPS-induced histologic injury is significantly reduced in mice receiving either an IV-

administered eNAMPT-neutralizing pAb (4mg/kg, at time 0 with LPS injection) (**center**) or the humanized ALT-100 mAb (**right**) (0.4mg/kg, at time 0 with LPS injection) (n= >5/group, *p<0.05 for LPS-Ab vs. LPS-PBS control, **p<0.05 for LPS-mAb vs. LPS-pAb). **B.** The ALT-100 mAb was significantly more effective than the eNAMPT pAb in reducing LPS-induced histologic evidence of inflammation and injury (*p<0.05 vs. LPS-PBS, **p<0.05 mAb vs. pAb). **C/D.** IV administration of either eNAMPT-neutralizing biologic intervention (pAb or mAb) significantly reduced LPS-induced increases in BAL protein (**C**) and BAL PMN counts (**D**) (*p<0.05 vs. LPS-PBS, **p<0.05 mAb vs. pAb). **E.** The superior efficacy of the humanized ALT-100 mAb compared to the eNAMPT pAb was again verified in an Acute Lung Injury Severity Score (ALISS) comprised of H & E staining, BAL protein, BAL PMN counts and IL-6 plasma levels (*p<0.01 vs. LPS-PBS, **p<0.01 mAb vs. pAb).

Figure 4. eNAMPT-neutralizing strategies attenuate "two-hit" preclinical ARDS/VILI injury. A. H&E lung tissue staining analysis in mice exposed to LPS (0.1mg/kg,18h) followed by mechanical ventilation (4h, tidal volume 20 mL/kg) **(left)** were histologically compared to control C57BL/6J mice (inset) revealing significant parenchymal neutrophil infiltration and both interstitial and alveolar edema. The severity of LPS/VILI histologic injury was significantly reduced in mice receiving either the eNAMPT-neutralizing polyclonal antibody (pAb, 4mg/kg, at time 0 with LPS) (**center**) or the humanized ALT-100 mAb (0.4mg/kg, at time 0 with LPS) (**right**). **B.** The ALT-100 mAb was significantly more effective than the pAb in reducing "two-hit" preclinical ARDS injury as captured by histologic quantification of injury (Image J software) (*p<0.05 vs.

LPS/VILI-PBS, **p<0.05 mAb vs. pAb). **C/D.** Both eNAMPT-neutralizing biologic interventions (pAb or mAb) also significantly reduced "two-hit" ARDS/VILI-induced increases in BAL protein content (**C**) and BAL PMN counts (**D**) after the "two-hit" LPS/VILI model (*p<0.05 vs. LPS/VILI-PBS, **p<0.05 mAb vs. pAb). **E.** Although both eNAMPT-neutralizing biologic interventions (pAb, mAb) significant reduced LPS/VILI inflammatory injury, the ALT-100 mAb proved more effective than the eNAMPT pAb as verified in the ALISS (n=5 mice/group) (*p<0.05 vs. LPS/VILI-PBS, **p<0.05 mAb vs. pAb).

Figure 5. eNAMPT-neutralizing strategies attenuate eNAMPT-induced human lung EC signaling and barrier responses. A/B. Human lung ECs were challenged with either human recombinant eNAMPT alone (1 ug/ml, 1h) or a eNAMPT-pAb antibody mixture (eNAMPT 1ug/ml + pAb 10 ug/ml, 1h). Cells were next lysed and probed for phospho-proteins and total β-actin via Western Blot. eNAMPT-induced robust phosphorylation of NFKB, in addition to evidence of MAP kinase activation (pp-p38, pp-JNK, pp-42/44 ERK). Heat-denatured (100^{o}C, 5 min) human recombinant eNAMPT (HD) (1 µg/ml, 1h) served as a negative control confirming that eNAMPT effects do not reflect endotoxin contamination. The addition of the eNAMPT-neutralizing pAb nearly totally abolished eNAMPT-induced NFkB phosphorylation and inhibited eNAMPT-induced MAP kinase activation detected by phosphorylation of ERK, p38, and JNK MAP kinases captured by densitometric measurements (n=3). **C.** In companion experiments, human lung ECs plated onto gold microelectrodes were challenged with either recombinant human eNAMPT alone (1 µg/ml), an eNAMPT-pAb mixture (eNAMPT 1ug/ml and pAb 10 ug/ml) or an eNAMPT-ALT-100 mAb mixture (eNAMPT 1ug/ml and

ALT-100 10 ug/ml). Both eNAMPT-neutralizing strategies, pAb, and mAb, attenuated eNAMPT-induced declines in EC barrier integrity compared to eNAMPT alone. Human lung ECs on gold microelectrodes were also challenged with LPS (1 µg/ml), with either PBS, eNAMPT pAb (10 µg/ml) or ALT-100 mAb (10 µg/ml) added immediately after LPS stimulation. The ALT-100 mAb, but eNAMPT pAb, also produced significant reductions in LPS-induced declines in EC barrier integrity compared to LPS alone. For TER studies, normalized resistance values >1 indicate lung EC barrier enhancement, normalized resistance values <1 indicate lung EC barrier disruption. **D.** Bar graph quantification of the TER declines and loss of barrier integrity, where data are expressed as change in TER compared to normalized unstimulated controls at 6h (± SEM, n=3 independent experiments per condition, *p<0.05 agonist alone versus agonist-pAb or mAb). **E.** Lung tissue homogenates from "one-hit" LPS-challenged (1mg/kg, 18h) with and without treatment with the eNAMPT-neutralizing mAb (0.4mg/kg at time 0h) were evaluated for Evans Blue Dye accumulation in lung tissues as a reflection of extravascular dye leakage and reported as the EBD concentration (µg/gram lung tissue) [58]. The bar graph demonstrates that the significant LPS-induced increases in EBD accumulation are abolished by prior addition of the ALT-10 mAb (*p<0.05 LPS vs. LPS + mAb).

Figure 6. The eNAMPT-neutralizing ALT-100 mAb attenuates MAP kinase signaling in "one-hit" and "two-hit" preclinical ARDS/VILI models. A. Lung tissue homogenates from "one-hit" LPS-exposed (1mg/kg, 18h) and "two-hit" LPS/VILI-exposed (LPS 22h; mechanical ventilation 4h, VT 20 mL/kg) C57B6 wild type mice were probed for phospho-proteins and total β-actin (Western Blot). LPS- and LPS/VILI-

challenged mice displayed robust NFkB and MAP kinase phosphorylation (pp-p38, pp-JNK, pp-42/44 ERK) as evidence of pathway activation. Treatment with the eNAMPT-neutralizing ALT-100 mAb (0.4mg/kg, at time 0h) resulted in signifiant reductions in both NFkB and MAP kinase pathway activation in the “one-hit”- and “two-hit” exposed mice captured by densitometric measurements **(Panel B)** (n=3)**.**

Figure 7. *EC-cNAMPT*$^{-/-}$ mice are significantly protected from lung injury in “one-hit” and “two-hit” ARDS injury models. A. Lung tissue sections were obtained from *EC-cNAMPT*$^{-/-}$ mice sacrificed >2 weeks post-initiation of tamoxifen treatment (75mg IP daily for 1 week) and tissue slides prepared for dual IHC staining with cell-specific double staining fluorescent-tagged NAMPT (green) and actin or CD-31 (red). In contrast to the dual staining in lung endothelium in littermate control sections (colocalized merge, **left**), tamoxifen-treated *EC-cNAMPT*$^{-/-}$ mice exhibit an absence of NAMPT staining in vascular cells while NAMPT staining in lung epithelium and leukocytes is prominent consistent with our original report [14]. These results reflect the targeted *NAMPT* deletion and absent expression in vascular endothelium. **B-D.** H&E staining of WT mice and *EC-cNAMPT*$^{-/-}$ mice exposed to the “one-hit” LPS ARDS model **(B**) or to the “two-hit” LPS/VILI model (**C**) demonstrates significantly reduced inflammatory lung injury in mice with conditional deletion of EC *NAMPT*, summarized by Image J quantification **(D)**. **E-G.** “One-hit” LPS- and “two-hit” LPS/VILI-exposed *EC-cNAMPT*$^{-/-}$ mice also exhibit significant reductions in BAL protein levels **(E)** and BAL PMN counts (**F)** with this protection captured in the integrated ALISS score (**G).** *$p<0.05$ *EC-cNAMPT*$^{-/-}$ vs similarly-exposed littermates.

Figure 8. EC NAMPT deletion and the ALT-100 mAb reduce plasma and tissue cytokine expression in "one-hit"- and "two-hit"-exposed ARDS mice. **A.** Plasma eNAMPT levels (ELISA) were significantly increased in "one-hit"- and "two-hit"-exposed littermate controls, with significantly reduced circulating eNAMPT levels in similarly exposed *EC-cNAMPT*$^{-/-}$ KO mice (*p<0.05 WT LPS or LPS-VILI vs. WT Ctrl, **p<0.05 *EC-cNAMPT*$^{-/-}$ vs "one-hit"/"two-hit"-exposed littermates). **B/C.** Plasma levels of the murine inflammatory cytokines, IL-6 and KC (IL-8) in "one-hit"- and "two-hit"-exposed *EC-cNAMPT*$^{-/-}$ KO mice are reduced levels compared to similarly-exposed littermates. **D.** Treatment with the eNAMPT-neutralizing humanized ALT-100 mAb reduces the increase in plasma levels of IL-6 in C57B6 wild type mice exposed to "one-hit" and "two-hit" preclinical ARDS injury models (*p<0.05 LPS or LPS/VILI alone vs. Ctrl, **p<0.05 LPS or LPS/VILI mAb vs. LPS or LPS/VILI alone). **E.** Western blot detection of IL-6 protein expression in lung tissue homogenates from "one-hit" LPS-exposed C57B6 wild type mice shows significant ALT-100 mAb-mediated reductions in IL-6 expression captured by densitometric measurements (n=4) (*p<0.05 LPS/VILI alone vs. Ctrl, **p<0.05 LPS/VILI mAb vs. LPS/VILI alone).

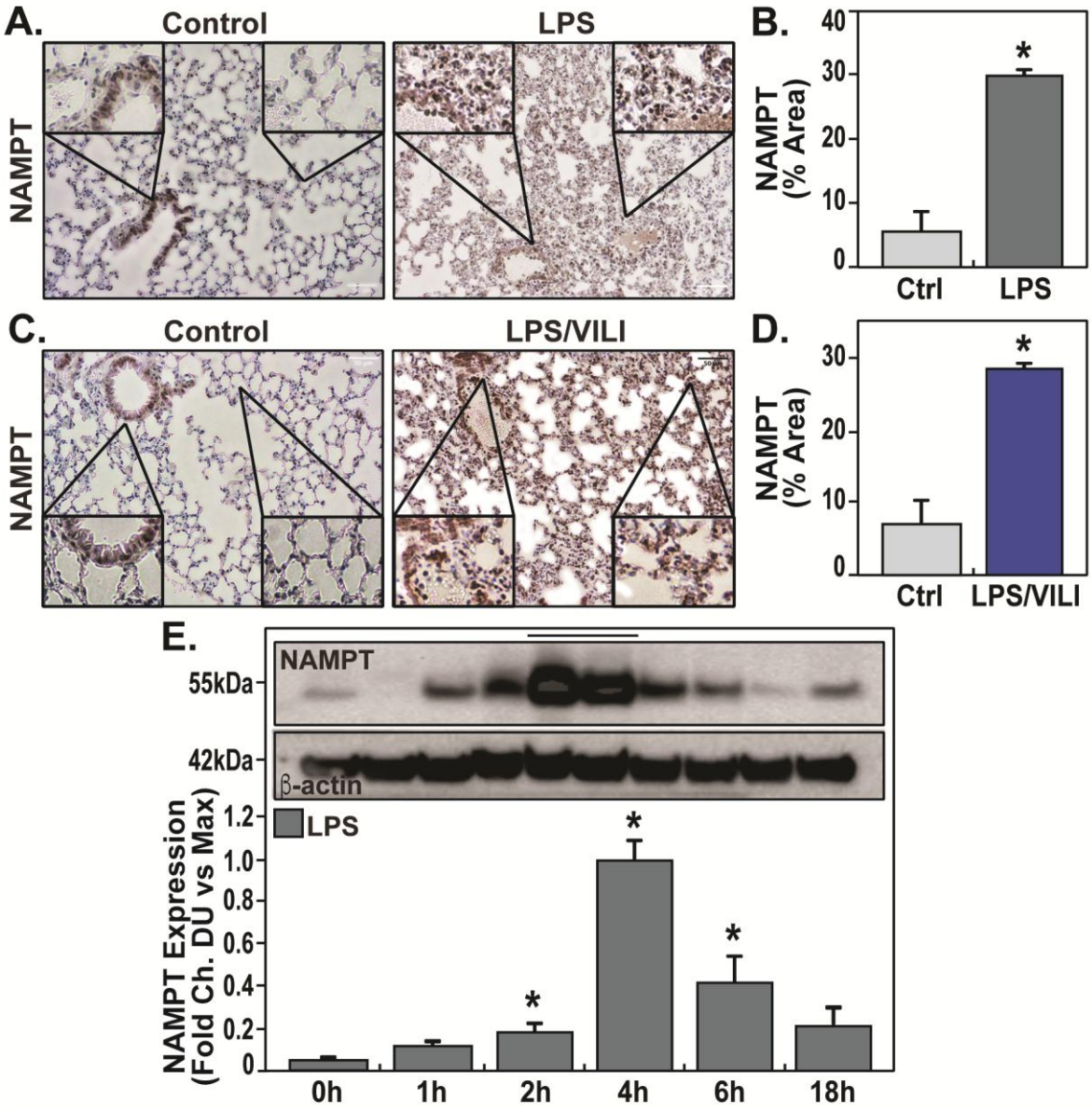
A.
Control
LPS
NAMPT
B.
NAMPT (% Area)
40
30
20
10
0
*
Ctrl
LPS
C.
Control
LPS/VILI
NAMPT
D.
NAMPT (% Area)
30
20
10
0
*
Ctrl
LPS/VILI
E.
NAMPT
55kDa
42kDa
β-actin
LPS
NAMPT Expression (Fold Ch. DU vs Max)
1.2
1.0
0.8
0.6
0.4
0.2
0
*
*
*
0h
1h
2h
4h
6h
18h

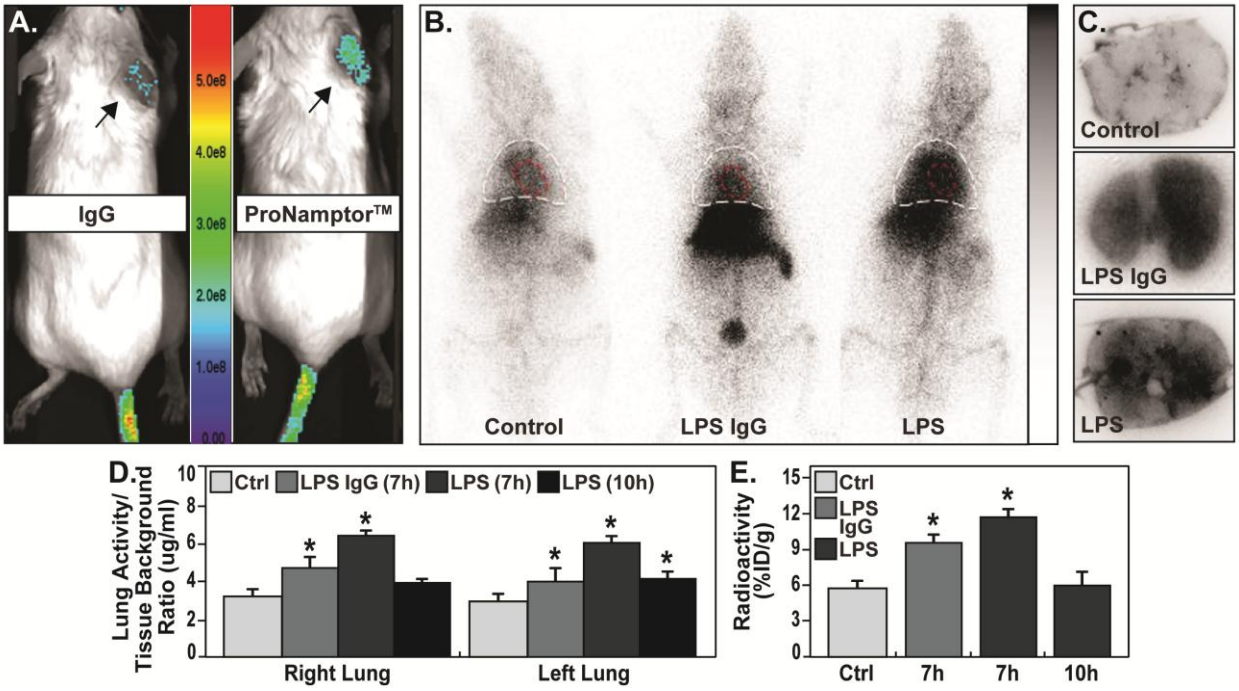
A.
IgG
ProNamptor™
5.0e8
4.0e8
3.0e8
2.0e8
1.0e8
0.00
B.
Control
LPS IgG
LPS
C.
Control
LPS IgG
LPS
D.
Lung Activity/ Tissue Background Ratio (ug/ml)
Ctrl
LPS IgG (7h)
LPS (7h)
LPS (10h)
Right Lung
Left Lung
E.
Radioactivity (%ID/g)
Ctrl
LPS IgG
LPS
Ctrl
7h
7h
10h

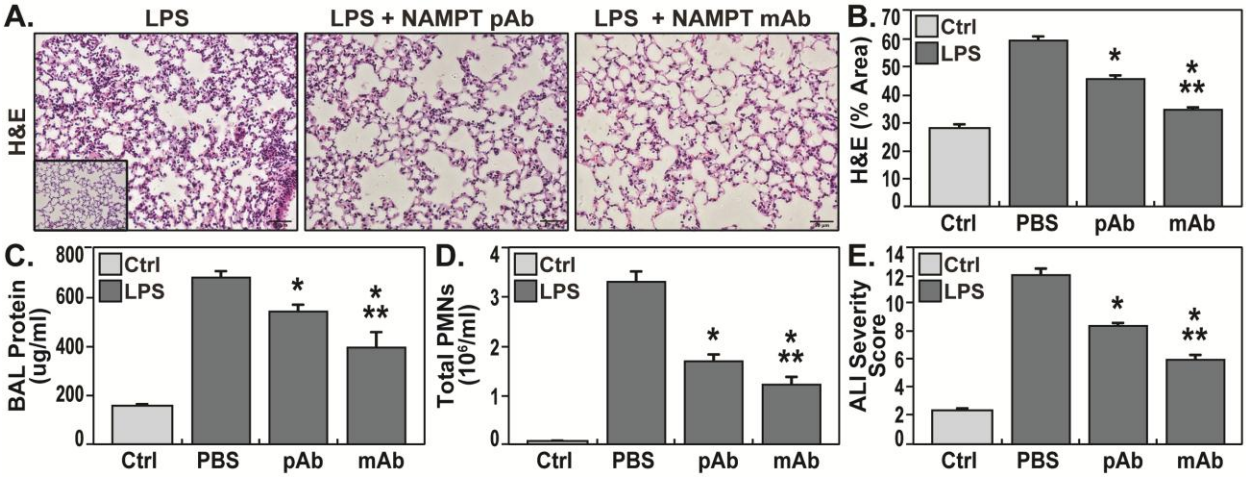
A.
LPS
LPS + NAMPT pAb
LPS + NAMPT mAb
H&E
B.
Ctrl
LPS
H&E (% Area)
70
60
50
40
30
20
10
0
*
**
Ctrl
PBS
pAb
mAb
C.
BAL Protein (ug/ml)
800
600
400
200
0
D.
Total PMNs (10^6/ml)
4
3
2
1
0
E.
ALI Severity Score
14
12
10
8
6
4
2
0

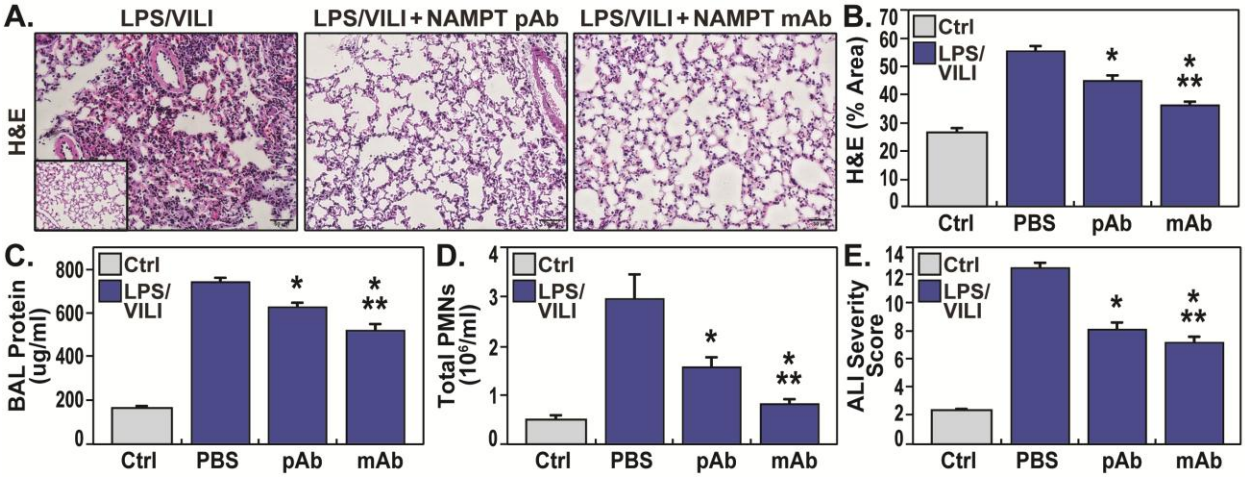
A.
LPS/VILI
LPS/VILI + NAMPT pAb
LPS/VILI + NAMPT mAb
H&E
B.
H&E (% Area)
Ctrl
LPS/VILI
Ctrl
PBS
pAb
mAb
C.
BAL Protein (ug/ml)
D.
Total PMNs (10^6/ml)
E.
ALI Severity Score
*
**

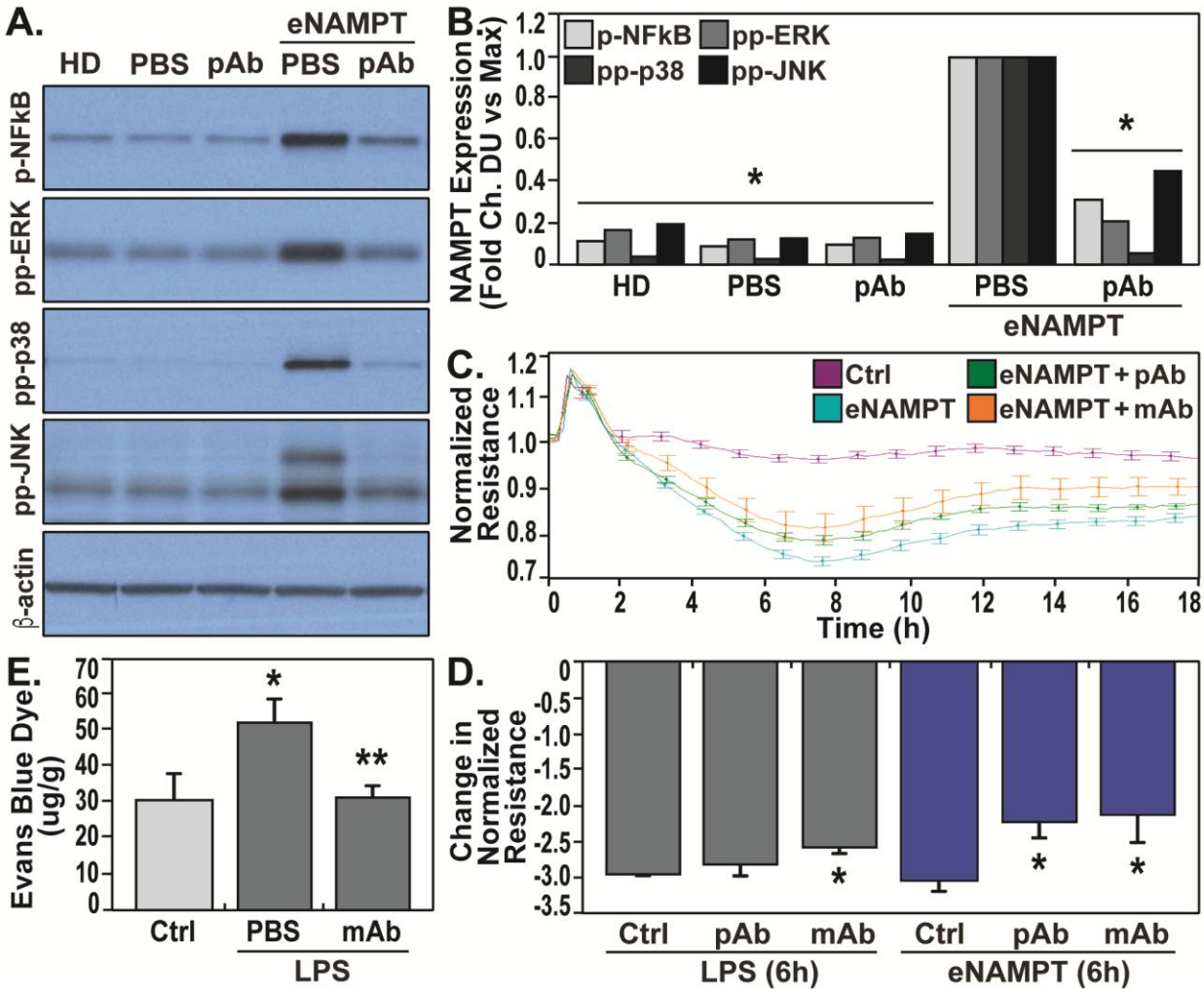
A.
eNAMPT
HD
PBS
pAb
PBS
pAb
p-NFkB
pp-ERK
pp-p38
pp-JNK
β-actin
B.
NAMPT Expression (Fold Ch. DU vs Max)
p-NFkB
pp-ERK
pp-p38
pp-JNK
HD
PBS
pAb
PBS
pAb
eNAMPT
C.
Normalized Resistance
Ctrl
eNAMPT
eNAMPT + pAb
eNAMPT + mAb
Time (h)
E.
Evans Blue Dye (ug/g)
Ctrl
PBS
mAb
LPS
D.
Change in Normalized Resistance
Ctrl
pAb
mAb
Ctrl
pAb
mAb
LPS (6h)
eNAMPT (6h)

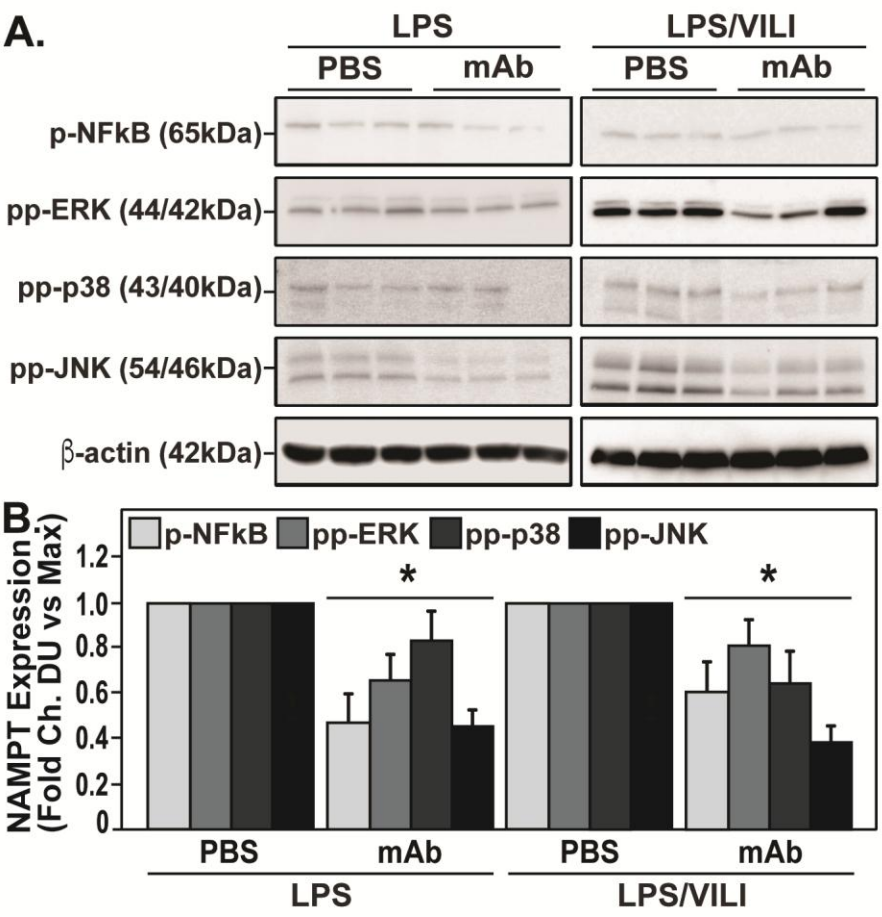
A.
LPS
LPS/VILI
PBS
mAb
PBS
mAb
p-NFkB (65kDa)
pp-ERK (44/42kDa)
pp-p38 (43/40kDa)
pp-JNK (54/46kDa)
β-actin (42kDa)
B
p-NFkB
pp-ERK
pp-p38
pp-JNK
NAMPT Expression
(Fold Ch. DU vs Max)
1.2
1.0
0.8
0.6
0.4
0.2
0
*
*
PBS
mAb
PBS
mAb
LPS
LPS/VILI

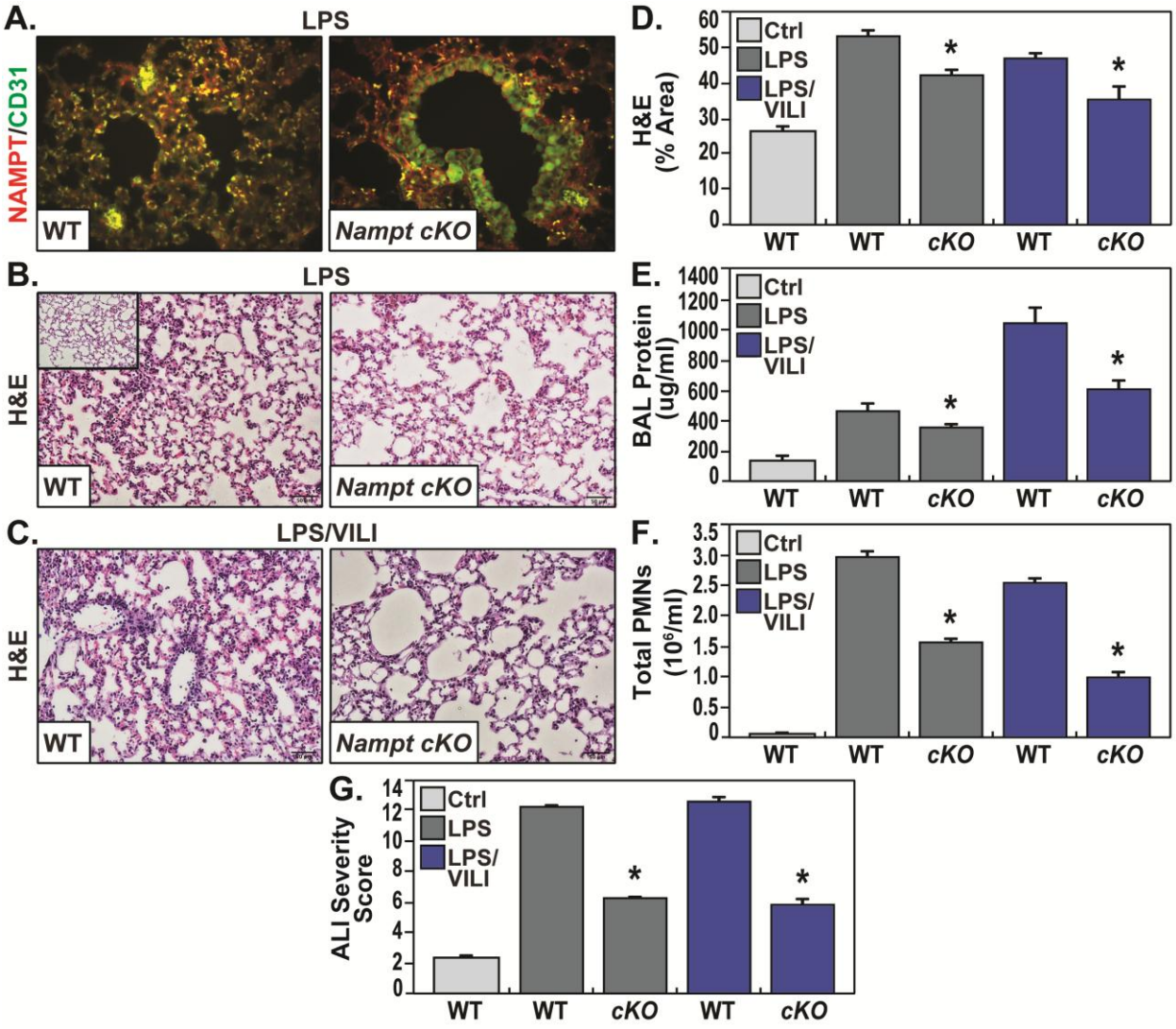
A.
LPS
NAMPT/CD31
WT
Nampt cKO
B.
LPS
H&E
WT
Nampt cKO
C.
LPS/VILI
H&E
WT
Nampt cKO
D.
H&E (% Area)
Ctrl
LPS
LPS/ VILI
WT
WT
cKO
WT
cKO
E.
BAL Protein (ug/ml)
F.
Total PMNs (10^6/ml)
G.
ALI Severity Score

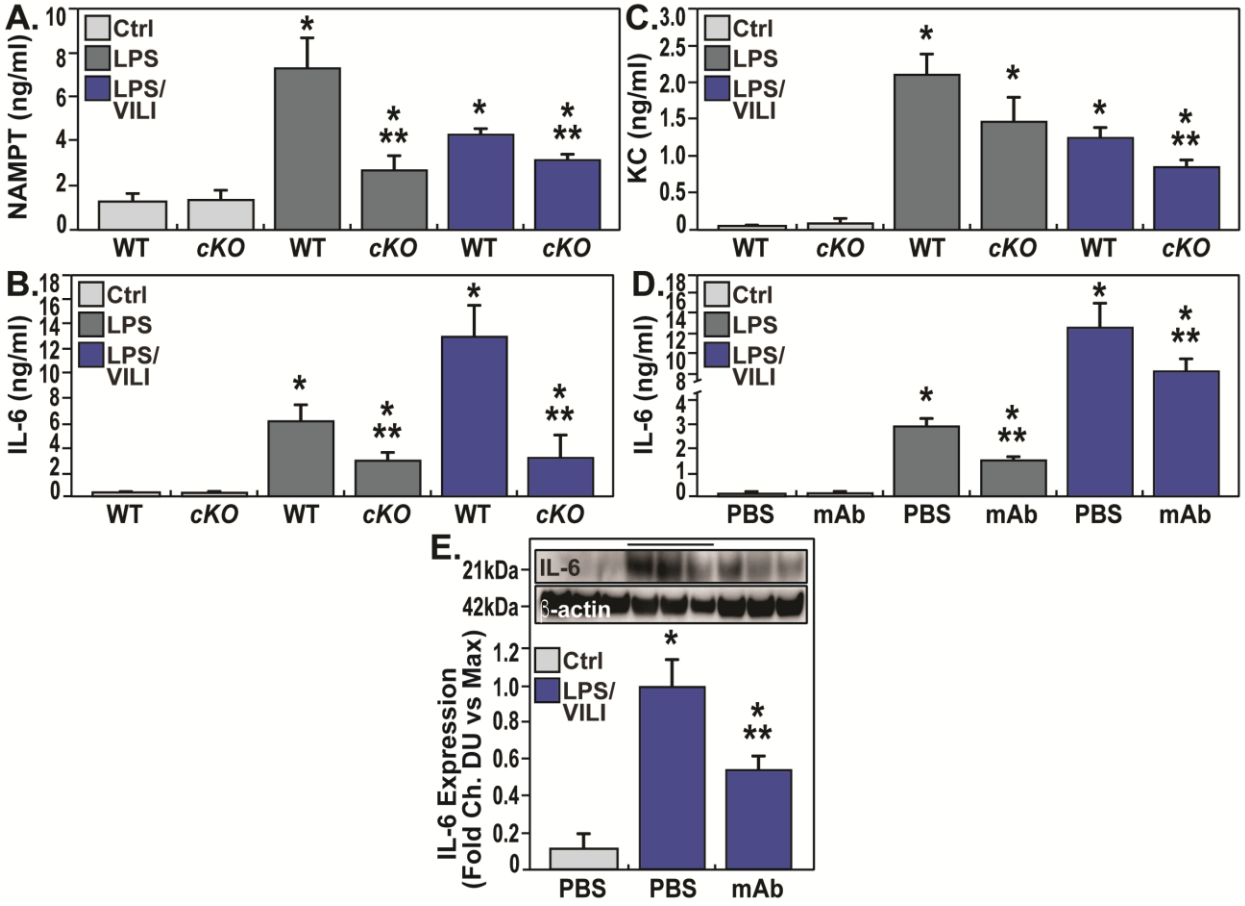
A.
NAMPT (ng/ml)
Ctrl
LPS
LPS/ VILI
WT
cKO
B.
IL-6 (ng/ml)
C.
KC (ng/ml)
D.
PBS
mAb
E.
21kDa
IL-6
42kDa
β-actin
IL-6 Expression (Fold Ch. DU vs Max)

Endothelial eNAMPT Amplifies Preclinical Acute Lung Injury: Efficacy of an eNAMPT-Neutralizing mAb

SUPPLEMENTAL MATERIALS AND METHODS

Reagents. Recombinant human eNAMPT was purchased from Peprotech (Cranbury, NJ). The following antibodies- p-NFkB, pp-ERK, pp-p38, pp-JNK, IL-6, IL-8 (KC)- were purchased from Cell Signaling Technologies (Danvers, MA); β-actin from Invitrogen (Carlsbad, CA) (NFkB); and goat, rabbit, and mouse secondary antibodies from Life Technologies (Waltham, MA). Goat anti-human NAMPT polyclonal antibody (pAb) was custom-generated (17) by Lampire Biological Laboratories, Inc. (Pipersville, PA) by immunizing against full length rhNAMPT protein. All other reagents, including lipopolysaccharides (LPS, E. Coli 0127:B8 strain), were from Sigma-Aldrich (St. Louis, MO), unless otherwise noted.

Generation of eNAMPT-neutralizing humanized monoclonal antibodies (mAbs). The eNAMPT-neutralizing humanized mAbs, ALT-100 and ALT-300 were provided by Aqualung Therapeutics Corporation (Tucson, AZ). ALT-100 and ALT-300 were derived from anti-human eNAMPT mAb-producing murine hybridomas (Abpro, Boston MA) which were extensively screened *in vitro* and *in vivo* and selected for high affinity eNAMPT binding and eNAMPT neutralization. Epitope-distinct murine mAbs (Abpro, Boston MA) from the two lead hybridomas underwent humanization (Fusion Antibodies, Belfast, UK) with generation of 50 humanized eNAMPT-neutralizing mAbs (25 mAbs per murine hybridoma). Each mAb was again screened *in vitro* using EC electrical resistance assays (34, 35), and NFkB activation biochemical assays (19) and by *in vivo* selection utilizing the preclinical murine lung injury models described below.

These screenings resulted in the selection of the three highest performing humanized mAbs (ALT-100, ALT-200, ALT-300). ALT-100 was selected for the *in vivo* therapeutic studies reported herein and ALT-300 chosen for incorporation into the tissue NAMPT-imaging probe, ProNamptor^{TM} for studies to probe tissue NAMPT expression as described below (^{99m}Tc-ProNamptor^{TM}). Extremely high NAMPT protein sequence homology between mice, rats, non-human primates and humans (95-99%), underscoring the utility of both the humanized ALT-100 and ALT-300 mAbs in the murine preclinical models reported in our studies.

Generation of the ProNamptor^{TM} mAb imaging probe. The ALT-300 eNAMPT-binding humanized mAb was used for generation of fluorescent and ^{99m}Tc-labeled probes for imaging NAMPT expression in tissues. A non-specific human IgG was also fluorescently- or ^{99m}Tc-labeled and used as a control to verify the uptake specificity of ALT-300. For Cy5.5 labeling, the Cy5.5-NHS was dissolved in dimethyl sulfoxide (DMSO) (5 µg/µL). The antibodies (1 mg/mL) in 0.1 M sodium bicarbonate buffer (pH 8.0) were reacted with Cy5.5-NHS at a molar ratio of 1:8. Following reaction in the dark (25C^{o}, 2 h), the reaction mixture was processed using Zeba™ Spin Desalting Columns (7K MWCO) (Thermo Fisher Scientific, Waltham, MA) to separate unbound dyes from the dye-conjugated antibody (36, 37).

^{99m}Tc-ProNamptor^{TM} was generated by radiolabeling ALT-300 with ^{99m}Tc by initial mAb conjugation with a heterobifunctional linker, succinimidyl-6-hydrazinonicotinate hydro-chloride (SHNH, in DMSO, 5 µg/µL) (Molecular Targeting Technologies, Inc., West Chester, PA) (36, 37) in 0.1 M sodium bicarbonate modification buffer (pH 8.0, 1:10 molar ratio, 25^{o}C, 2 h). The SHNH-conjugated product (SHNH-antibody) was

purified and buffer-exchanged by conjugation buffer (100 mM sodium phosphate, 150 mM sodium chloride, pH 6.0) using the Zeba™ Spin Desalting Columns. Radiolabeling was completed by additions of $^{99m}TcO_4^-$ (15-20 mCi, 0.4-0.5 mL saline), Tricine solution (30 µL, 36 mg/mL), Tin(II) chloride dihydrate (10 µL, 2 mg/ml) in 0.1N HCl, and SHNH-antibody conjugate (16 µL, 100 µg) in 0.1M PBS pH 6.0 (25°C, 30 min). ^{99m}Tc-ProNamptor™ was purified using a G-25 Sephadex column and the radiochemical purity (RCP) was determined by size-exclusion high performance liquid chromatography (SEC-HPLC). The radiolabeling yield of ^{99m}Tc-ProNamptor™ was consistently greater than 90%. After gel filtration purification, all ^{99m}Tc-ProNamptor™ preparations used for animal injections exhibited greater than 98% RCP. In addition, a human IgG ^{99m}Tc probe was generated and served as control for the ^{99m}Tc-ProNamptor experiments.

^{99m}Tc-ProNamptor™ mAb imaging. A mouse model of skin inflammation induced by topical application of 12-O-tetradecanoylphorbol-13-acetate (TPA) was utilized to validate the ability of the Cy5.5-ALT-300 probe to detect NAMPT tissue expression *in vivo* (38, 39). Ear edema was induced in mice (10-15 weeks old) by topical application of 2 µg TPA dissolved in 20 µL of acetone, and administered through a micropipette to the inner and outer surface of the right ear (10 µL) with repeated application at 24 hours. The left ear was treated with 20 µL of acetone (vehicle) applied topically as a negative control. Three hours following the second TPA application, either Cy5.5-eNamptor™ or Cy5.5-IgG (15-20 µg) was injected intravenously (n=3 mice) and imaged (Lago Bioluminescence and Fluorescence Imaging System, Spectral Instruments Imaging, Tucson, AZ).

To assess the capacity of the ^{99m}Tc-ALT-300 probe to detect *in vivo* NAMPT tissue expression, ^{99m}Tc-ProNamptor^{TM} (1.0-1.5 mCi, >98% radiochemical purity, 40, 41) was intravenously injected into two groups of C57BL/6J mice (n=3 each group) at 3h and 7h post intratracheal LPS instillation, i.e. the "one-hit" LPS ARDS model described in detail,below. An additional group received saline as a vehicle control (n=6). Mice were imaged at 30 min, 120 min and 240 min after radiotracer injection using a Quantum Imaging Detector (iQID) camera (42-44). This small-animal imaging system provides imaging of photon and particle emissions in small animals and tissues with high spatial resolution. After completion of the imaging, all mice were euthanized and the lungs were harvested for count activity-based measurements of ^{99m}Tc-ProNamptor^{TM} biodistribution and for *ex vivo* autoradiography.

Mouse studies. *In vivo* experiments utilized either wild type male C57BL/6J mice (8–12 weeks, Jackson Laboratories, Bar Harbor, ME), EC-specific conditional *NAMPT* knockout mice *(EC-cNAMPT$^{-/-}$)* on a mixed 129/B6 background, or littermate NAMPT$^{fl/fl}$ controls. All mice were housed under standard conditions (12h light-dark cycle, 25-27°C, ~40% humidity) in autoclaved micro-isolator cages with free access to food and water. All animal care procedures and experiments were approved by the Institutional Animal Care and Use Committee (University of Arizona). For the "one-hit" preclinical ARDS injury experiments, mice were challenged with LPS for 18h. For the "two-hit" preclinical ARDS injury experiments, mice were exposed to LPS for 18h with mechanical ventilation for the last 4 hours as we have described previously (46-48). In specific experiments, C57BL/6J mice received either intravenously-delivered PBS (vehicle control), a eNAMPT-neutralizing polyclonal antibody (pAb, 4mg/kg), or a

humanized eNAMPT-neutralizing monoclonal antibody (ALT-100 mAb, 0.4mg/kg) via the jugular vein.

Generation of conditional *NAMPT* knockout mice *(EC-cNAMPT$^{-/-}$)*. Utilizing the University of Arizona Genetically-Engineered Mouse Model (GEMM) Core, a floxed *NAMPT* mouse was created (*NAMPT$^{fl/fl}$*). Briefly, a targeting vector was generated with a loxP site in intron 1, a FRT-flanked neo-containing positive selection cassette in intron 2, and second loxP site downstream of the neo-cassette. A thymidine kinase-negative selection cassette was inserted into intron 3. The targeting vector was electroporated into 129/S6 ES cells and selected for G418 resistance and gancyclovir sensitivity and the targeted ES cells injected into B6D2xB6 blastocysts. Positive expressing offspring were confirmed with the following genotyping primers: TCGAGCTATCATCATGCTTAACTTAC (common F), AAATCCCTCAGTGCACAGTAAATAG (wildtype R), CTGGCACTCTGTC GATACCC (neo R) creating band lengths of 244 bp (wildtype) and 372 bp (flox). *NAMPT$^{fl/fl}$* were in-crossed to produce mice homozygous for the floxed allele which were then crossed with a tamoxifen-inducible EC-specific Cre transgenic mouse line (Tek-cre/ERT2-1Soff) to create *EC-cNAMPT$^{-/-}$* mice (45), Mice were then backcrossed with the floxed homozygous *NAMPT* mouse to create an EC-specific conditional *NAMPT* KO mouse (*EC-cNAMPT$^{-/-}$*). To induce Cre activity, mice were injected for 5 consecutive days with tamoxifen (Sigma Aldrich) at a dose of 75mg/kg tamoxifen in corn oil. All *EC-cNAMPT$^{-/-}$* mice were utilized for experimentation after a minimum wait of two weeks after the final dose of tamoxifen. Mice were maintained on a mixed 129/B6 background and littermates that did not express the Cre recombinase gene were used as controls.

EC-specific KO mice carrying the NAMPT flox transgene did not display discernible differences in phenotypic traits compared to their wild-type littermates. Growth rates, fecundity, and fertility also did not differ from wild-type mice. Similarly, *NAMPT* flox mice crossed with the TIE2/ERT2 Cre mice to generate the conditional *NAMPT* KO line did not exhibit any phenotypic differences from either littermates or parental strains, both before and after tamoxifen injections.

Preclinical "one-hit" and "two-hit" preclinical ARDS models of LPS- and ventilator-induced murine lung injury. Mice were anesthetized by an intraperitoneal injection of a mixture of ketamine (100 mg/kg) and xylazine (5 mg/kg) with additional doses given as needed to ensure adequate anesthetic depth. Animals were intubated with a 20-G angiocatheter and received intratracheal LPS injection (*E. Coli* 0127:B8, 1 mg/ kg) with harvesting 18h ("one-hit" lung injury model). For the "one-hit" ARDS model, mice received an intratracheal LPS injection followed sacrificing at 18h as previously described (46-48). For the "two-hit" LPS/VILI-induced lung injury model, animals received intratracheal LPS (0.1 mg/kg) and after 18hrs, were reintubated and placed on mechanical ventilation for 4h (Advanced Ventilator System For Rodents, SAR-1000, CWE Incorporated, Ardmore, PA) as previously described (46-48). Mice were ventilated with room air for 4h using the following parameters: tidal volume (VT) 20 ml/kg, respiratory rate 90 breaths/min, and positive-end expiratory pressure 0 cm H_2O. Spontaneously breathing (SB) control animals were intubated and received intratracheal PBS but allowed to breathe spontaneously on room air during the duration of the experiment.

eNAMPT-neutralizing strategies in "one-hit" and "two-hit" preclinical ARDS models. Concomitantly with LPS challenge in either the "one-hit" or the "two-hit" model, specific groups of C57BL/6J mice received either an eNAMPT-neutralizing goat pAb (Lampire) or the humanized mAb (Aqualung Therapeutics, Tucson AZ) via i.v. injection (4mg/kg or 0.4mg/kg, respectively). An additional pAb or mAb dose was provided prior to the onset of mechanical ventilation in the LPS/ VILI " two-hit" model.

Bronchoalveolar lavage (BAL) analysis. At the termination of each experiment, mice were euthanized by IACUC-approved exsanguination after anesthesia. BAL was performed with 1 ml of cold Hank's buffered saline solution (HBSS) (Invitrogen) delivered intratracheally followed by slow recovery of the fluid as we have previously described (49). BAL fluid underwent centrifugation (500*g*, 20 min, 4°C), pellets re-suspended in 200µL cold HBSS and 1mL of RBC Lysis Solution (5 min). The pellet was recentrifuged (500*g*, 10 min, 4°C) and re-suspended in 200µL cold HBSS for total cell counting via an automated cell counter (TC20; Bio-Rad, Hercules, CA). PMN determinations were performed as previously described (49) by assessing the % of PMNs in BAL cytospins and multiplying by the total number of BAL cells retrieved/mL. The BAL supernatant was re-centrifuged (16,500g, 10 min, 4°C), and the supernatant collected for total protein measurements (Pierce BCA Protein Assay Kit, Thermo Scientific). BAL supernatant was stored at -80°C for further analysis.

Lung histology and immunohistochemistry (IHC) analyses. Hematoxylin and eosin staining: To assess alterations in the lung tissue morphology, lungs were fixed in 10% neutral buffered formalin for a minimum of 48 h, embedded in paraffin, sectioned and stained with hematoxylin-eosin (H & E). Routine H&E slides were

prepared using Richard-Allan hematoxylin, clarifier, bluing reagent and eosin and imaged (Olympus digital camera, 10x magnification) (50). **NAMPT staining:** The avidin-biotin-peroxidase method utilized a rabbit anti-human NAMPT polyclonal antibody (dilution of 1:1000, Bethyl Laboratories, Inc, Montgomery, TX) for IHC staining to visualize NAMPT expression in lung tissues (5 micron sections) as previously described (14, 17, 19). Results were compared to a rabbit IgG control (matched protein concentration, 1ug/ml, Vector Labs, Burlingame CA). Deparaffinized and rehydrated slides were ringed with an ImmunoPen rinsed in TBS, blocked for endogenous peroxidase (0.5% hydrogen peroxide, 20 min) and protein blocked (Vector Labs, 1 h, avidin D and biotin block, Vector Labs, 25^0C). Slides were incubated overnight (4^oC) in primary or IgG control followed by application of the biotinylated secondary Ab (1 h) with incubation with avidin-biotin complex (Vector Labs, 40 min, 25^0C). The protein was visualized using DAB plus nickel (Vector Labs, 4 min) and counterstained with Mayers hematoxylin (Newcomer Supply, Middleton, WI) and bluing reagent added (Richard-Allan Scientific, San Diego CA). **NAMPT/CD31 co-staining in *EC-cNAMPT*$^{-/-}$ mice**: Formalin-fixed, paraffin-embedded lung tissue sections from *EC-cNAMPT*$^{-/-}$ mice were baked at 65^oC overnight, washed in xylene (to remove paraffin), and passed through 100%, 75%, 50% isopropanol, and $_{dd}$H20 for rehydration. Antigen retrieval was performed using a sodium citrate buffer [10 mM sodium citrate, 0.05% Tween 20, pH 6.0] and heated at 97^oC using decloaking chamber for 20 min. Slides were washed in washing buffer (0.1 M Tris-HCl, 0.3 M NaCl, 0.1% Tween 20, and 7.7 uM NaN3, pH 7.6 at 25^oC) followed by blocking buffer (5% v/v normal bovine serum, 0.1 M Tris-HCl, 0.15 M NaCl, pH 7.6, 25^oC, 30 min). Slides were next incubated overnight (4^oC) with primary

rabbit anti-human NAMPT pAb (Bethyl Laboratories, Montgomery, TX) or the rat monoclonal anti-CD31 antibody (AbCam Cambridge, MA, #7388, MEC 7.46), diluted in blocking buffer in a humidified chamber. Slides were next washed 3 times in wash buffer and incubated with biotinylated secondary antibody (1h, 25^{o}C, washed 3 times in washing buffer, mounted using ProLong Diamond Antifade Mountant (Thermo Fisher Scientific, P36970) and stored in the dark (25^{o}C) to cure the mountant. Specimens were imaged using Zeiss Axiovert Photomicroscope using a 10X objective (NA 0.4).

Evans Bue Dye extravasation assay: We evaluated lung vascular leakage by measuring extravascular Evans Blue Dye in the lung. Briefly, mice were injected Evans blue dye (0.05 mg, Sigma) i.v. 60 min before euthanasia. Lungs were then perfused to remove the intravascular dye, excised and homogenized in PBS. One volume of lung homogenate was incubated with 2 volumes of formamide and incubated at 60°C for 18 hrs before centrifugation. The optical density of the supernatant was measured at 620 nm and 740 nm using an Imark microplate reader. Concentrations of Evans blue were corrected for the presence of heme pigments using the following formula: A_{620} (corrected) = A_{620} (raw)—(1.1927 X A_{720}) + 0.0071 (58). The extravasated Evans blue dye concentrations were then calculated against a standard linear curve as a reflection of vascular protein leak into lung tissues.

Quantitative histologic analyses. Histological images from each group captured with light microscopy (Olympus digital camera) at 10x magnification, were randomly selected for quantification of H&E and NAMPT staining using ImageJ software (51) (different sections of each slide). For H&E image analysis, the percentage of area selected for measurement with all images processed and stored for statistical analysis.

For NAMPT staining image analysis, color segmentation plugin was utilized with POINTCROSS tool applied to each NAMPT staining image with a total of 3 color clusters. The area percentage of each color cluster was recorded and saved for statistical analysis.

Acute Lung Injury Severity Score (ALISS) quantification. The Acute Lung Injury Severity Score (ALISS) was utilized to integrate lung injury indices in the "one-hit" and "two-hit" preclinical ARDS models and to standardize the injury levels across the *in vivo* models. A ranking point system, incorporating published recommendations (59) objectively assigns a score to each study animal (1 to 4 points) for each of 4 injury severity readouts (H & E histology quantification, BAL total protein concentration, BAL total PMN cell count and plasma levels of the pro-inflammatory cytokine IL-6). The maximal score for each animal is 16 points/mouse. In general, an ALISS score of 1-4 reflects the complete absence of injury, scores of 5-8 points reflect mild injury, scores of 9-12 points reflect moderate injury, and scores >12 points reflect severe injury.

Measurements of electrical resistance across human lung endothelial cells-Trans-endothelial Electrical Resistance (TER). Human pulmonary artery endothelial cells (HPAEC or ECs) were obtained from Lonza (Walkersville, MD) and cultured as we described previously (52) in the manufacturer's recommended endothelial growth medium-2 (EGM-2). Cells (passages 6 to 9) were seeded onto evaporated gold microelectrodes in polycarbonate wells and grown to confluence (37°C, 5% CO_2). Trans-endothelial electrical resistance (TER) measurements were performed using an electrical cell-substrate impedance sensing system (Applied Biophysics, Troy, NY) as we have described previously in detail (53). Cells were monitored over time for TER

responses to agonist stimulation. TER values from each microelectrode were pooled as discrete time points and plotted versus time as the mean ± SEM.

Biochemical tissue expression of NAMPT, NFkB, MAP kinases and IL-6. Western blotting of lung homogenates obtained from "one-hit"- and "two-hit"-exposed mice was performed according to standard protocols as previously reported (23, 49). Lung tissues were homogenized in radioimmunoprecipitation assay lysis buffer (RIPA buffer) (20 mM Tris-HCl, pH 7.4, 150 mM NaCl, 1 mM EGTA, 1 mM β-glycerophosphate, 1 mM Na_3VO_4, 1 % NP-40, 1% sodium deoxy-cholate, 1 µg/ml leupeptin, and 10 µg/ml protease inhibitors- 1mM AEBSF, 800nM aprotinin, 50 µM bestatin, 15 µM E64, 20 µM leupeptin, 10 µM pepstatin A). Following homogenization, lysates were centrifuged (12,000 rpm, 10 min, 4^{o}C) and equal amounts of protein (40 µg) loaded onto 4-12% Bis Tris gels (Life Technologies). Western blotting was performed according to standard protocols (21, 47). Lung tissue expression levels of NAMPT, NFkB, MAP kinases, IL-6, and β-actin (total protein control) with densitometric quantification of lung tissue expression.

Murine plasma levels of eNAMPT by ELISA. eNAMPT plasma levels were measured in plasma by ELISA as we have previously reported (27, 31). Briefly, a 96-well plate (Nunc MaxiSorp) coated with proprietary goat anti-NAMPT pAb (100 uL/well, 8 µg/ml, diluted in coating buffer (1.5 g Na2CO3, 2.93 g NaHCO3 /1L distilled water, pH 9.6). After 24 h (4^{o}C) the plate was warmed to 37^{o}C (1 h), washed in 1x TBST (3 times, 0.1%) and incubated with 1% BSA-TBS (100 uL/well, 1 h, 37^{o}C) to reduce non-specific binding. The plate was again washed with 1x TBS-T, followed by incubation with either the human rhNAMPT standard or the murine plasma sample diluted 1/10 in plasma

diluent buffer (100 uL/well) (Cygnus). The plate was again incubated overnight (4^{o}C), warmed 37^{o}C, and washed 3 times in 1x TBS-T. To detect plasma eNAMPT, the plate was incubated with the rabbit anti-NAMPT pAb (Bethyl, 100 uL/well, dilution 1:10,000 in 1% BSA-TBS) for 1 h at 37^{o}C followed by washing 3 times in 1x TBS-T. The plate was next incubated with the secondary donkey anti-rabbit HRP-labelled pAb (100 uL/well, 1:10,000 in 1% BSA-TBS) at 37^{o}C for 1 h, followed by 1x TBS-T washing. The plate was finally developed with the HRP substrate (SIGMAFAST OPD) for 5 min at 25^{0}C with the reaction stopped with 10% H2SO4, followed by absorbance reading 490 nm.

Murine plasma inflammatory cytokine levels via meso scale discovery (MSD) platform. A meso-scale ELISA platform was utilized (Meso Scale Diagnostics, Rockville, MD) for measurements of plasma levels of IL-6 and IL-8 (KC). Each biotinylated antibody (10 µg/ml, specific for each analyte, was mixed with a different linker for each analyte and incubated for 30 min at 25^{0}C. The reaction was terminated with 200 µl of free biotin solution and 600 µl of the 10x U-PLEX linked biotinylated antibody solution with 50 µl of coating solution was added to each well in 96 well plate and incubated for 1 h (800 rpm shaking, 25^{0}C). After washing, each well was supplemented with 25 µl of diluent and 25 µl of calibrator or samples/standards, incubated for 1 h (800 rpm shaking, 25^{0}C). After washing (TBS-T), each well was supplemented with 50 µl/well of 1x detection antibody solution, again incubated for 1h, washed and supplemented with 2x Read Buffer T followed by plate imaging and calculation of the absolute concentration values based on standards.

Statistical analysis. Continuous data were compared using nonparametric methods and categorical data by chi square test. Where applicable, standard one-way

ANOVA was used and groups compared using the Newman-Keuls test. Two-way ANOVA was used to compare the means of data from two or more different experimental groups. If a significant difference was present by ANOVA ($p < 0.05$), a least significant differences (LSD) test was performed post hoc. Statistical tests were performed using GraphPad Prism version 7.00 for Windows, GraphPad Software, La Jolla California USA, www.graphpad.com. Statistical significance was considered at $p < 0.05$.

Supplemental Figure 1

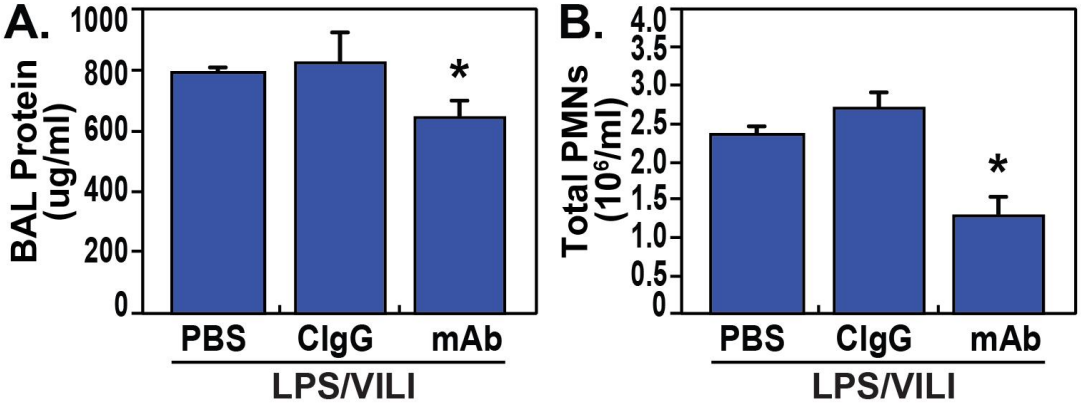

Supplemental Figure 1. The specific eNAMPT-neutralizing mAb, but not a non-specific human IgG, attenuates "two-hit" preclinical ARDS/VILI injury. The significant increases in BAL protein **(Panel A)** and BAL PMNs **(Panel B)** in mice exposed to LPS (0.1mg/kg,18h) followed by mechanical ventilation (4h, tidal volume 20 mL/kg) were significantly reduced in mice receiving the eNAMPT-neutralizing humanized ALT-100 mAb (0.4mg/kg, at time 0 with LPS) but not injection of **non-specific human IgG antibody** (*$p<0.05$ vs. LPS/VILI-PBS).